

# Error analysis of linear optics measurements via turn-by-turn beam position data in circular accelerators

A. Franchi  
*ESRF, Grenoble, France*  
 (Dated: April 18, 2018)

Many advanced techniques have been developed, tested and implemented in the last decades in almost all circular accelerators across the world to measure the linear optics. However, the greater availability and accuracy of beam diagnostics and the ever better correction of linear magnetic lattice imperfections (beta beating at 1% level and coupling at 1‰) are reaching what seems to be the intrinsic accuracy and precision of different measurement techniques. This paper aims to highlight and quantify, when possible, the limitations of one standard method, the harmonic analysis of turn-by-turn beam position data. To this end, new analytic formulas for the evaluation of lattice parameters modified by focusing errors are derived. The unexpected conclusion of this study is that for the ESRF storage ring (and possibly for any third generation light source operating at ultra-low coupling and with similar diagnostics), measurement and correction of linear optics via orbit beam position data are to be preferred to the analysis of turn-by-turn data.

## I. INTRODUCTION AND MOTIVATION

Measurement and correction of focusing errors in circular accelerators is one of the top priorities in colliders and storage ring-based light sources to provide users with beam sizes and divergences as close as possible to the design values and to limit the possible detrimental effects on the beam lifetime caused by the integer and half-integer resonances. To this end, so many different techniques have been developed and successfully tested since decades that they already occupy entire chapters in textbooks [1].

A brief and non-exhaustive historical overview may help understand the great advancements in this domain. Back to the early '80s, one of the first measurements of betatron phase advance and beta functions was documented in Ref. [2]. In the early '90s systematic measurements and correction were already carried out at the CERN Large Electron Positron (LEP) collider from the harmonic analysis of turn-by-turn (TBT) beam position monitor (BPM) data, reaching a beta beating of 10% [3, 4]. In the first decades of the new century other colliders worldwide reported similar or even lower modulation [5–7]. With the advent of 3rd generation light sources, a major breakthrough was provided by the exploitation of orbit BPM data for the reconstruction of machine errors [8, 9], resulting in modulation of the beta functions from 10% down to 1% or even less in more recent facilities.

The ever increasing BPM resolution and computing power made the analysis and correction of linear optics (focusing error and betatron coupling) via measurements of the orbit response matrix (ORM) a routine task in basically all light sources worldwide. The inclusion of TBT features in the BPM electronics and the refinement of the data analysis via several model-independent techniques [10, 11] provided these facilities with a viable alternative tool. However, systematic comparisons between these two techniques on the same machine ap-

peared only recently (for the ALBA and SOLEIL storage rings) [12, 13]: While both approaches evaluated the measured beta beating in the 1% – 2% range with respect to the ideal model, they differed of about the same quantity when compared against each other. Systematic numerical simulations on the same lattice showed indeed that the expected resolution of both approaches is of about 1% [13, 14].

These observations fostered an intense debate (mostly oral, during workshops, conferences or informal meetings) on a series of questions: *i)* Which is the best approach to measure the linear optics at 1% level of beta beating? *ii)* Why do the two methods predict different modulations of the optics functions and fail to converge toward the same model? *iii)* Which is the ultimate resolution at which lattice errors can be measured and corrected? The community split in two main schools of thoughts. The ORM-oriented group argues that the higher BPM resolution of the orbit mode with respect to the TBT setup provides the most reliable observable (the ORM) and that the inferred model best reproducing it can be trusted for the evaluation (and correction) of the lattice parameters. The TBT-oriented school replies that TBT data can be trusted more in the evaluation of beta beating and betatron phase errors because these quantities are more direct observables, whereas their measurements result from a series of model-dependent fits when orbit data are used.

This paper aims to help answer the above questions. Even though the scrutiny of TBT data is limited here to the harmonic analysis, the general final conclusions are expected to apply to other approaches, such as the BPM matrix, the 1-turn or N-turn matrix. Each aspect is quantified here by using the ESRF electron storage ring as example: Even though numbers may vary in other facilities, the overall considerations should apply to other machines with similar level of ultra-low coupling, diagnostics and beam stability. On the other hand, hadron machines are not expected to be subjected to the same

conclusions, because their nonlinearities are weaker than in modern light sources, i.e. they have a larger area in the  $x$ - $y$  plane within the linear regime of the betatron motion compared to storage rings like the ESRF's. Moreover, analytic error estimates are derived here for the TBT analysis only. No equivalent results are obtained for the ORM approach, for which the only error study presently available is based on the same numerical parametric scans of Ref. [14]. The scope of this comparison is also limited to the analysis of lattice errors without entering into the field of different correction schemes. The analysis of practical considerations which may prevent some facilities from using either technique is also out of the scope of this paper, which is organized as follows. After briefly reviewing the main physical and mathematical ingredients behind the two approaches in Sec. II, a more detailed discussion on the validity of approximations and assumptions proper of each method under typical measurement conditions is presented in Sec. III. Consequences for the present and future ESRF storage rings are eventually outlined in Sec. IV. All mathematical derivations have been put in separated appendices.

## II. CURRENT APPROACHES TO THE ANALYSIS OF LINEAR OPTICS ERRORS

As mentioned in the Introduction, two main strategies are implemented in circular accelerators for the analysis of linear lattice errors. The first, which is routinely used in probably all synchrotron-based light sources, is based on the examination of the orbit response to a steering angle. The second focuses on the analysis of free betatron oscillations induced by a pulsed excitation and is the preferred one in hadron circular accelerators.

In the first approach, after introducing an orbit distortion via horizontal and vertical deflections, represented by two vectors  $\vec{\Theta}_x = (\Theta_{x,1}, \Theta_{x,2}, \dots, \Theta_{x,N_S})$  and  $\vec{\Theta}_y = (\Theta_{y,1}, \Theta_{y,2}, \dots, \Theta_{y,N_S})$ , where  $N_S$  is the number of available magnets, the horizontal and vertical orbits are recorded at  $N_B$  BPMs  $\vec{O}_x = (O_{x,1}, O_{x,2}, \dots, O_{x,N_B})$  and  $\vec{O}_y = (O_{y,1}, O_{y,2}, \dots, O_{y,N_B})$ . They can be written as

$$\begin{pmatrix} \vec{O}_x \\ \vec{O}_y \end{pmatrix} = \mathbf{ORM} \begin{pmatrix} \vec{\Theta}_x \\ \vec{\Theta}_y \end{pmatrix}, \quad \mathbf{ORM} = \begin{pmatrix} \mathbf{O}^{(xx)} & \mathbf{O}^{(xy)} \\ \mathbf{O}^{(yx)} & \mathbf{O}^{(yy)} \end{pmatrix},$$

$$O_{wj}^{(xx)} = \frac{\partial O_{x,j}}{\partial \Theta_{x,w}}, \quad O_{wj}^{(xy)} = \frac{\partial O_{x,j}}{\partial \Theta_{y,w}}, \quad 1 < j < N_B, \quad (1)$$

$$O_{wj}^{(yx)} = \frac{\partial O_{y,j}}{\partial \Theta_{x,w}}, \quad O_{wj}^{(yy)} = \frac{\partial O_{y,j}}{\partial \Theta_{y,w}}, \quad 1 < w < N_S$$

Optics codes such as MADX [17] or AT [18] can easily compute **ORM** for the ideal (or initial) lattice model and the difference between the measured and expected matrix may be written as

$$\delta \mathbf{ORM} = \mathbf{ORM}^{(\text{meas})} - \mathbf{ORM}^{(\text{ideal})}. \quad (2)$$

The horizontal and vertical dispersion are also measured and their difference with respect to the ideal model is

computed

$$\delta \vec{D}_{x,y} = \vec{D}_{x,y}^{(\text{meas})} - \vec{D}_{x,y}^{(\text{ideal})}. \quad (3)$$

Both  $\delta \mathbf{ORM}$  and  $\delta \vec{D}_{x,y}$  depend linearly on the linear lattice errors (i.e. from bending and quadrupole magnets). By sorting the elements of each ORM block sequentially in a vector, the dependence reads

$$\begin{pmatrix} \delta \vec{O}^{(xx)} \\ \delta \vec{O}^{(yy)} \\ \delta \vec{D}_x \end{pmatrix} = \mathbf{M}_{\text{norm}} \begin{pmatrix} \delta \vec{K}_1 \\ \delta \vec{K}_0 \end{pmatrix}, \quad (4)$$

$$\begin{pmatrix} \delta \vec{O}^{(xy)} \\ \delta \vec{O}^{(yx)} \\ \delta \vec{D}_y \end{pmatrix} = \mathbf{M}_{\text{skew}} \begin{pmatrix} \vec{\theta}^{(\text{quad})} \\ \vec{\theta}^{(\text{bend})} \end{pmatrix}. \quad (5)$$

$\delta \vec{K}_1$  and  $\delta \vec{K}_0$  are the vectors containing the quadrupole and dipole errors, respectively, whereas  $\vec{\theta}$  refers to the magnet tilts. The latter may be replaced in Eq. (5) by the corresponding skew multipolar components

$$J_1 = -K_1 \sin(2\theta^{(\text{quad})}), \quad J_0 = -K_0 \sin(\theta^{(\text{bend})}). \quad (6)$$

Throughout the paper, the MADX nomenclature for the multipolar expansion of magnetic fields is adopted,

$$- \Re \left[ \sum_n (K_{w,n-1} + iJ_{w,n-1}) \frac{(x_w + iy_w)^n}{n!} \right], \quad (7)$$

with  $K$  and  $J$  referring to the integrated normal and skew magnetic strengths. The response matrices  $\mathbf{M}_{\text{norm}}$  and  $\mathbf{M}_{\text{skew}}$  can be computed by the optics codes. By pseudo-inverting the above system, for instance via singular value decomposition (SVD), effective models that best fit the measured ORM can be built. A unique model may not be extracted, since a trade-off between accuracy (i.e. large number of eigen-values in the decomposition) and reasonableness of the errors (i.e. low number of eigen-values to prevent numerical instabilities) shall be fixed on a subjective base. Moreover, the systems of Eqs. (4)-(5) ignores contributions from the feed-down effects of quadrupoles and sextupoles induced by their misalignments and/or off-axis orbit at their locations. The closed orbit distortion resulting from this modelling renders the analysis more complex without adding values to the physical observables (betatron phase  $\phi$  and amplitude  $\beta$  at the BPMs) and are usually *absorbed* by additional dipole errors (accounting for quadrupole misalignments) and quadrupole errors (representing the quadrupolar feed-down in sextupoles). In optics codes dipole errors induce a distortion of the reference orbit, though not of the closed one. Eqs. (4)-(5) are the core of the *Linear Optics from Closed Orbit* (LOCO) analysis [8, 9]. Additional fit parameters may be included in the r.h.s. of the two equations, such as calibration factors and rolls of steerers and BPMs. Once the errors ( $\delta \vec{K}_1$ ,  $\delta \vec{K}_0$  and  $\vec{\theta}$ ) are included into the lattice model, the optical parameters ( $\beta$ ,  $\phi$  and  $D$ ) are computed by

the optics codes and compared to the ones from the ideal model. Beta beating and phase advance errors are the most common figures of merit for focusing errors:

$$\frac{\Delta\beta}{\beta} = \frac{\beta^{(meas)} - \beta^{(mod)}}{\beta^{(mod)}}, \quad (8)$$

$$\delta\phi_{ij} = \Delta\phi_{ij}^{(meas)} - \Delta\phi_{ij}^{(mod)}, \quad \Delta\phi_{ij} = \phi_j - \phi_i$$

where both quantities are evaluated at the BPM locations, with  $i$  and  $j$  two different monitors, usually (though not necessarily [19]) consecutive. A consensus on a figure of merit for the evaluation of betatron coupling has not yet been reached. In hadron machines the amplitude of the difference resonance stop-band  $|C|$  is widely used, [1]

$$C = -\frac{1}{2\pi} \oint ds j(s) \sqrt{\beta_x(s)\beta_y(s)} e^{-i(\phi_x(s) - \phi_y(s)) + i(s/R)\Delta Q},$$

where  $j(s)$  represents the distribution of the non-integrated skew quadrupole fields along the ring,  $R$  is the machine radius,  $s$  is the longitudinal coordinate,  $\beta$  and  $\phi$  are the Twiss parameters of the uncoupled lattice, and  $\Delta Q = Q_x - Q_y$  the fractional distance from the resonance of the set tunes.  $|C|$  evaluated on the resonance ( $\Delta Q = 0$ ) corresponds to the minimum separation experienced by the measured eigen-tunes  $|\Delta Q_{min}|$  [20]. In lepton circular accelerators the ratio between the two transverse emittances  $\epsilon_r = \epsilon_y/\epsilon_x$  is preferred, since any measurable value of  $\epsilon_y$  is usually generated by betatron coupling and vertical dispersion. Both  $|C|$  and  $\epsilon_r$  are global parameters that prevent a detailed localisation and compensation of sources of coupling in light sources. To this end, in Ref. [22] the coupling resonance driving terms (RDTs) were proposed as figure of merit along with vertical dispersion,

$$f_{1010, j}^{1001} = \frac{\sum_w J_{w,1} \sqrt{\beta_{w,x}\beta_{w,y}} e^{i(\Delta\phi_{x,wj} \mp \Delta\phi_{y,wj})}}{4(1 - e^{2\pi i(Q_u \mp Q_v)})} + O(J_1^2). \quad (9)$$

$J_{w,1}$ ,  $w = 1, 2, 3, \dots, W$  are the skew quadrupole integrated strengths present in the ring and originated by quadrupole tilts, sextupole misalignments, insertion devices, and corrector skew quadrupoles already powered.  $\beta_w$  is the beta function at the source of coupling  $w$ , while  $\Delta\phi_{wj}$  denotes its phase advance with respect to the BPM  $j$ .  $Q_{u,v}$  are the measurable eigen-tunes, which are, in first approximation, equal to the set tunes:  $Q_{u,v} = Q_{x,y} + O(J_2^2)$ .  $\Delta\phi_{wj}$  is the phase advance between the source of coupling  $w$  and the BPM  $j$  where the RDTs are computed. These two RDTs can be evaluated (and minimized) at all BPMs from the model obtained after fitting the measured ORM and used to evaluate (and reduce) the vertical emittance along the ring, as shown in Ref. [22].

The second approach is based on the harmonic analysis of turn-by-turn (TBT) free betatron oscillations induced

by a pulsed magnet. Forced oscillations generated for example by an AC dipole are not discussed here. However, to the first order, and provided that the AC dipole driving frequency is sufficiently separated from the tune, the following analysis can be applied to both signals, either free or forced. At each BPM, the TBT signal can be decomposed in its main harmonics via a Fourier transform. The main harmonic is found at a frequency corresponding to the tune, whereas secondary harmonics appear at linear combinations of both tunes,  $n_x Q_x + n_y Q_y$ , with  $n_{x,y} \in \mathbb{N}$ , as reported in Fig.7 of Ref. [23]. Spectral lines in the horizontal and vertical planes are usually denoted as  $H(n_x, n_y)$  and  $V(n_x, n_y)$ , respectively. The tune lines at the BPM  $j$  read

$$H(1, 0)_{j,\beta} = C_{x,j} \sqrt{2I_x \beta_{x,j}^{(meas)}} \cos(2\pi N Q_x + \phi_{x,j}^{(meas)} + \psi_{x0})$$

$$V(0, 1)_{j,\beta} = C_{y,j} \sqrt{2I_y \beta_{y,j}^{(meas)}} \cos(2\pi N Q_y + \phi_{y,j}^{(meas)} + \psi_{y0})$$

$\psi_0$  is an arbitrary initial phase equal for all BPMs (provided that the latter are perfectly synchronized in time),  $N$  is the turn number,  $\phi_j^{(meas)}$  is the BPM betatron phase and  $2I$  is the invariant (i.e. the action) proportional to the strength of the pulsed excitation. The BPM calibration factor  $C_j$  is added to account for values potentially different from 1. By performing the harmonic analysis on the TBT signal normalized by the model beta function, the horizontal tune line reads

$$\tilde{x}_j = \frac{x_j}{\sqrt{\beta_{x,j}^{(mod)}}} \rightarrow \frac{H(1, 0)_{j,\beta}}{\sqrt{\beta_{x,j}^{(mod)}}} = H(1, 0)_j, \quad (10)$$

$$H(1, 0)_j = C_{x,j} \sqrt{2I_x \frac{\beta_{x,j}^{(meas)}}{\beta_{x,j}^{(mod)}}} \cos(2\pi N Q_x + \phi_{x,j}^{(meas)} + \psi_{x0}).$$

An equivalent expression applies to the vertical plane. At the ESRF the same filtered and interpolated Fast Fourier Transform (FFT) of Ref. [24] is used to extract amplitude and phase of this harmonic, namely

$$\begin{cases} |H(1, 0)_j| = \frac{1}{2} C_{x,j} \sqrt{2I_x \frac{\beta_{x,j}^{(meas)}}{\beta_{x,j}^{(mod)}}} \\ \Phi_{H(1,0)_j} = \phi_{x,j}^{(meas)} + \psi_{x0} \end{cases}, \quad (11)$$

The invariant may be inferred by averaging the tune line amplitude over all BPMs, provided that their number and location are sufficient to cancel the contribution of the modulation of beta function and calibration factors,

$$\sqrt{2I_x} \simeq 2 < |H(1, 0)| >, \quad \sqrt{2I_y} \simeq 2 < |V(0, 1)| >. \quad (12)$$

The actual beta functions  $\beta^{(meas)}$  can be extracted from Eqs. (11)-(12), according to

$$\beta_{x,j}^{(meas)} \simeq \beta_{x,j}^{(mod)} \left( \frac{|H(1, 0)_j|}{< |H(1, 0)| >} \right)^2 \frac{1}{C_{x,j}^2}$$

$$\beta_{y,j}^{(meas)} \simeq \beta_{y,j}^{(mod)} \left( \frac{|V(0, 1)_j|}{< |V(0, 1)| >} \right)^2 \frac{1}{C_{y,j}^2}. \quad (13)$$

The uncomfortable dependence on the calibration factors in the above formulas motivated the search for an alternative way to extract  $\beta^{(meas)}$  from the tune line. The BPM phase  $\Phi$  of Eq. (11) turns out to be independent of both  $\mathcal{C}$ , BPM rolls and betatron coupling. Because of this robustness,  $\Phi$  was used in Ref. [3] to derive a different formula. The first observation is that the betatron phase advance  $\Delta\phi_{ij}$  between two BPMs is equal to the difference of the tune line phases, namely

$$\begin{aligned}\Delta\Phi_{H,ij} &= \Phi_{H(1,0)_j} - \Phi_{H(1,0)_i} = \Delta\phi_{x,ij} \\ \Delta\Phi_{V,ij} &= \Phi_{V(0,1)_j} - \Phi_{V(0,1)_i} = \Delta\phi_{y,ij}\end{aligned}, \quad (14)$$

the initial phases  $\psi_{x0,y0}$  of Eq. (10) canceling out. By assuming that the region between three BPMs is free from unknown focusing errors, the following formula was derived in Ref. [3] to compute the beta function at the first BPM from the measured and model phase advances between three monitors:

$$\beta_1^{(meas)} = \beta_1^{(mod)} \frac{\cot \Delta\phi_{12}^{(meas)} - \cot \Delta\phi_{13}^{(meas)}}{\cot \Delta\phi_{12}^{(mod)} - \cot \Delta\phi_{13}^{(mod)}}. \quad (15)$$

The above relation applies to both transverse planes and is independent of any BPM calibration factor and roll. Even though originally conceived to work on three consecutive BPMs, it provides more robust results if several sets of triplets are used to apply Eq. (15) first, and the corresponding beta functions are properly averaged after, as shown in Ref. [19].

As far as betatron coupling is concerned, the same RDTs of Eq. (9) can be measured independently only if the harmonic analysis is performed on the complex signal of the Courant-Snyder (C-S) coordinates  $\tilde{x} - i\tilde{p}_x$  (and  $\tilde{y} - i\tilde{p}_y$ ) [23], whereas the harmonic analysis discussed here is carried out on the real signals  $\tilde{x}$  ( $\tilde{y}$ ) of Eq. (10). The momentum  $\tilde{p}$  can be inferred by combining the position data of two BPMs [29] under the assumption that the invariant is constant between the two monitors. The presence of sextupoles and higher-order multipoles between two BPMs does alter the invariant, though this change is a higher order deformation that should not affect the linear analysis. On the other hand, the presence of coupling sources introduces a partial exchange of the two betatron invariants  $2I_{x,y}$  [21]. This introduces a systematic error in the reconstruction of the momenta  $\tilde{p}_{x,y}$ , which is proportional to the coupling RDTs (i.e. to the unknown quantity to be measured), with the risk of corrupting the analysis of the betatron coupling. In Ref. [23] it is shown that combined coupling RDTs,  $F_{xy}$  and  $F_{yx}$  can be measured at each BPM  $j$  from the two coupling harmonics of  $\tilde{x}$  and  $\tilde{y}$ , i.e.  $H(0,1)$  and  $V(1,0)$ , respec-

tively:

$$\begin{cases} F_{xy,j} = f_{1001,j} - f_{1010,j} \\ F_{yx,j} = f_{1001,j}^* - f_{1010,j}^* \\ |F_{xy,j}| = |H(0,1)_j| / (2|V(0,1)_j|) \mathcal{C}_{y,j} / \mathcal{C}_{x,j} \\ |F_{yx,j}| = |V(1,0)_j| / (2|H(1,0)_j|) \mathcal{C}_{x,j} / \mathcal{C}_{y,j} \\ q_{F_{xy,j}} = \arg\{H(0,1)_j\} - \frac{3}{2}\pi - \arg\{V(0,1)_j\} \\ q_{F_{yx,j}} = \arg\{V(1,0)_j\} - \frac{3}{2}\pi - \arg\{H(1,0)_j\} \end{cases}, \quad (16)$$

where the possible dependence on the BPM calibration factors has been made explicit. In (hadron) machines where  $|f_{1010}| \ll |f_{1001}|$ ,  $F_{xy} \simeq F_{yx}^* \simeq f_{1001}$  and a calibration-independent formula to measure the amplitude of the RDT reads [25]

$$|f_{1001}| \simeq \frac{1}{2} \sqrt{\frac{|H(0,1)||V(1,0)|}{|H(1,0)||V(0,1)|}}. \quad (17)$$

### III. LIMITS OF THE CURRENT APPROACHES

#### A. ORM analysis: model-dependent and time-consuming

The retrieval of lattice parameters from the analysis of the closed orbit requires twice the employment of the computer lattice model: first in the fit of the measured ORM, Eqs. (4)-(5), then in computation of the new lattice parameters for the evaluation of beta beating and phase advance errors of Eq. (4). Moreover, the analysis of orbit data is sensitive to BPM calibration factors, though effective coefficients can be inferred during the analysis of the ORM. This strong dependence on the initial lattice model, along with numerical issues related to possible degeneracies between fitting parameters, is considered by some as an intrinsic weakness of the ORM analysis.

Another drawback of the ORM analysis is its lengthy procedure for a single measurement and analysis. The acquisition typically foresees a sequence of current changes in orbit correctors and the retrieval of the corresponding orbit data. In the ESRF storage ring, this phase takes about 10 minutes for a partial ORM (32 out of 192 steerers), or 1 hour for a complete one. In larger machines such as the Large Hadron Collider (LHC) of CERN the time needed to scan the entire magnetic cycle makes this approach unsuitable for operational purposes. However, a new approach making use of alternating current steerers, fast BPM acquisition system (at 10 kHz) and harmonic analysis of orbit data was proved to obtain the same measurement with simultaneous magnet excitations at different frequencies, hence reducing dramatically the measurement time [16]. Still, superconducting machines like the LHC may not benefit from this variation. The analysis too is quite time consuming, since the



responses  $\mathbf{M}_{\text{norm}}$  and  $\mathbf{M}_{\text{skew}}$  of the ORM on the lattice errors ( $\delta K$ s and  $\theta$ s) in Eqs. (4)-(5) is computed by simulating an ORM for each error: A heavy computation already for the ESRF storage ring with 256 quadrupoles and 64 dipoles, which can only become more lengthy in larger machines and future light sources.

### B. TBT analysis: error analysis of Eq. (15)

Efforts have been made in the last three decades to conceive measurement techniques (as much as possible) independent of the initial computer model. Eq. (15) was derived in the 90s along with other handy expressions for the reconstruction of lattice parameters from TBT data in a way to be independent of the BPM calibration factors [3]. Moreover, the dependence on the initial model was smartly limited optics functions only (i.e. of  $\beta^{(meas)}$  starting from  $\beta^{(mod)}$  and  $\Delta\phi^{(mod)}$ ). The Model Independent Analysis (MIA) of Ref. [10, 26, 27] and the more recent Independent Component Analysis (ICA) of Ref. [11, 28] proposed a statistical approach to extract the same lattice parameters with no *a priori* knowledge of the initial model. All these advancements were successfully applied to many circular accelerators across the world. However, the autonomy from the initial model to fit and/or interpret the measured TBT data comes to the price of *forcing* the description of the same data according to some hypothesis, assumptions or approximations, of which more will be said in Sec. III F.

As mentioned in the previous section, Eq. (15) assumes that no quadrupole error is present between the three BPMs. In Appendix A an extension of that formula not requiring this hypothesis is derived up to the first order in the field errors  $\delta K_1$ :

$$\beta_1^{(meas)} = \beta_1^{(mod)} \frac{\cot \Delta\phi_{12}^{(meas)} - \cot \Delta\phi_{13}^{(meas)}}{\cot \Delta\phi_{12}^{(mod)} - \cot \Delta\phi_{13}^{(mod)} + (\bar{h}_{12} - \bar{h}_{13})} + O(\delta K_1^2) \quad , \quad (18)$$

$$\bar{h}_{ij} = \mp \frac{\sum_{i < w < j} \beta_w^{(mod)} \delta K_{w,1} \sin^2 \Delta\phi_{wj}^{(mod)}}{\sin^2 \Delta\phi_{ij}^{(mod)}} \quad , \quad (19)$$

where the sum runs over all quadrupole errors between the BPMs  $i$  and  $j$ . The sign depends on the plane: negative for  $x$ , positive for  $y$ .

If no error is present between the three BPMs, Eq. (15) is retrieved as expected. A special case where this equation still applies even in the presence of strong localized focusing errors is when  $\bar{h}_{13} = \bar{h}_{12} \neq 0$ . More generally, it remains a robust approximation whenever the beating induced by the quadrupole errors between three BPMs has a minor impact on the cotangent of their phase advance,  $|\bar{h}_{13} - \bar{h}_{12}| \ll |\cot \Delta\phi_{13}^{(mod)} - \cot \Delta\phi_{12}^{(mod)}|$ , or when it is much smaller than the one generated by focusing glitches

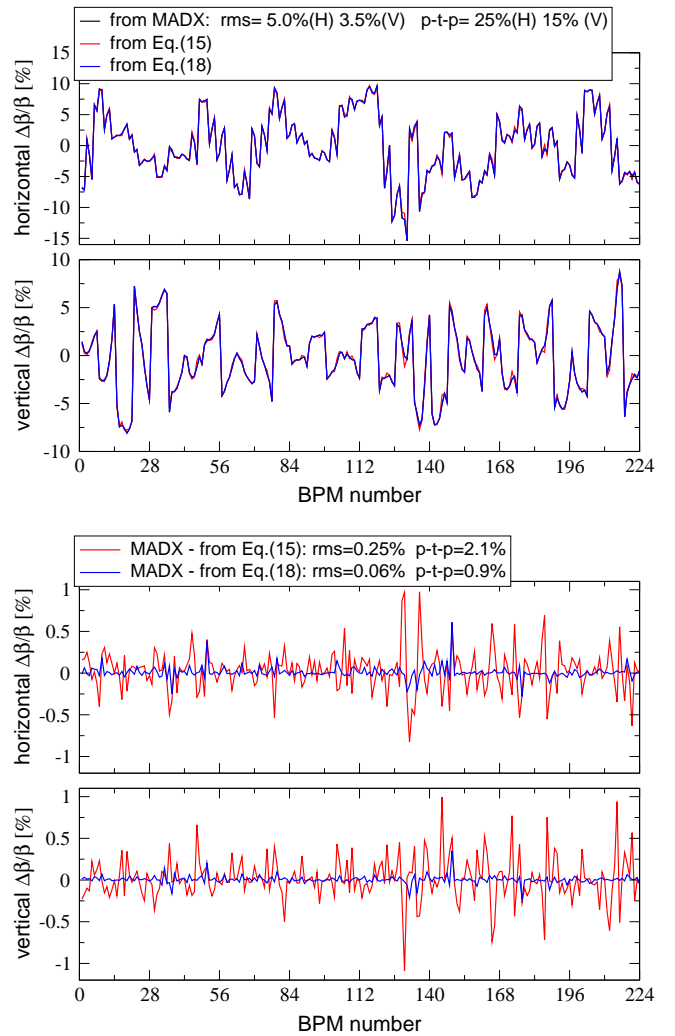


FIG. 1. (Color) Top: Beta beating induced by a typical set of errors in the ESRF storage ring as computed by MADX and the two formulas Eqs. (15) and (18). *rms* stands for “root-mean square”, *p-t-p* for “peak-to-peak”. Bottom: difference between the real beating (MADX) and one obtained from two formulas: In this example, the new Eq. (18) is four times more accurate than Eq. (15). A pity  $\bar{h}_{ij}$  is not observable and Eq. (18) may not be used for measurements!

along the rest of the ring, see discussion after Eq. (A33) of Appendix A.

In the upper plot of Fig. 1 an example is shown with the beta beating computed for a typical set of linear lattice errors in the ESRF storage ring. The beating is first computed by MADX, then the BPM phase advances are used to evaluate it with the existing formulas of Eq. (15), and eventually the  $\bar{h}_{ij}$  are also calculated from the model and applied to Eq. (18). The latter turns out to be more accurate than the former (see bottom plot of Fig. 1). Unfortunately, Eq. (18) is of no help in improving the measurement of the beta beating, since  $\bar{h}_{ij}$  is not an observable. However, once the error model is built, it can be computed *a posteriori* and used to estimate the accuracy (i.e. systematic error bars) of the direct measurement via

Eq. (15), which reads

$$\frac{\delta\beta_{meas}}{\beta} = \frac{\beta_{Eq.(15)} - \beta_{Eq.(18)}}{\beta_{Eq.(18)}} \simeq \frac{\bar{h}_{13} - \bar{h}_{12}}{\cot \Delta\phi_{12}^{(mod)} - \cot \Delta\phi_{13}^{(mod)}}. \quad (20)$$

An interesting feature of the above expression is that it depends on the ideal lattice parameters ( $\phi^{(mod)}$  and  $\beta^{(mod)}$ ) and the field deviations  $\delta K_1$  only. Hence it does not require the evaluation of the new optics induced by the errors. This may accelerate the estimation of the systematic errors from the statistical analysis of various error distributions along large rings, as in Ref. [19].

In the derivation of Eq. (18), other handy formulas for the evaluation of C-S parameters modified by focusing errors have been obtained,

$$\left\{ \begin{array}{l} \beta_{x,j} \simeq \beta_{x,j}^{(mod)} (1 + 8\Im\{f_{2000,j}\}) \\ \alpha_{x,j} \simeq \alpha_{x,j}^{(mod)} (1 + 8\Im\{f_{2000,j}\}) - 8\Re\{f_{2000,j}\} \\ \Delta\phi_{x,ij} \simeq \Delta\phi_{x,ij}^{(mod)} - 2h_{x,ij} + 4\Re\{f_{2000,j} - f_{2000,i}\} \end{array} \right., \quad (21)$$

$$\left\{ \begin{array}{l} \beta_{y,j} \simeq \beta_{y,j}^{(mod)} (1 + 8\Im\{f_{0020,j}\}) \\ \alpha_{y,j} \simeq \alpha_{y,j}^{(mod)} (1 + 8\Im\{f_{0020,j}\}) - 8\Re\{f_{0020,j}\} \\ \Delta\phi_{y,ij} \simeq \Delta\phi_{y,ij}^{(mod)} - 2h_{y,ij} + 4\Re\{f_{0020,j} - f_{0020,i}\} \end{array} \right.,$$

where the focusing RDTs  $f_{2000}$  and  $f_{0020}$  are defined in Eqs. (A2) and (A36), while explicit expressions for the detuning coefficients  $h_{ij}$  can be found in Eq. (A18). Even though the RDTs are complex quantities, only their real ( $\Re$ ) and imaginary ( $\Im$ ) parts enter in the above equations, whose remainders are proportional to  $f^2$ .

### C. TBT analysis: error analysis of Eq. (13)

In Appendix A, a more general version of Eq. (13) is derived, namely

$$\left\{ \begin{array}{l} \beta_{x,j}^{(meas)} = \beta_{x,j}^{(mod)} \left( \frac{|H(1,0)_j|}{\langle |H(1,0)| \rangle} \right)^2 \times \\ \quad [1 + 2(\langle \mathcal{E}_x \rangle - \mathcal{E}_{x,j}) + O(\mathcal{E}_x^2)] \times \\ \quad [1 + 64 \langle |f_{2000}|^2 \rangle + O(|f_{2000}|^3)] \\ \beta_{y,j}^{(meas)} = \beta_{y,j}^{(mod)} \left( \frac{|V(0,1)_j|}{\langle |V(0,1)| \rangle} \right)^2 \times \\ \quad [1 + 2(\langle \mathcal{E}_y \rangle - \mathcal{E}_{y,j}) + O(\mathcal{E}_y^2)] \times \\ \quad [1 + 64 \langle |f_{0020}|^2 \rangle + O(|f_{0020}|^3)] \\ \mathcal{C}_{x,y} = 1 + \mathcal{E}_{x,y} \quad , \quad 0 \simeq \mathcal{E}_{x,y} \ll 1 \end{array} \right., \quad (22)$$

where  $\langle |f|^2 \rangle$  and  $\langle \mathcal{E} \rangle$  represent the averaged values (over all BPMs) of the amplitudes of focusing RDTs squared and calibration errors, respectively. Unless these are determined by independent measurements, they cannot be disentangled and are not observable. A (rude)

zero-order truncation is then needed in order to apply Eq. (22) to real data, yielding to

$$\left\{ \begin{array}{l} \beta_{x,j} = \beta_{x,j}^{(mod)} \left( \frac{|H(1,0)_j|}{\langle |H(1,0)| \rangle} \right)^2 + O(\mathcal{E}_x, |f_{2000}|^2) \\ \beta_{y,j} = \beta_{y,j}^{(mod)} \left( \frac{|V(0,1)_j|}{\langle |V(0,1)| \rangle} \right)^2 + O(\mathcal{E}_y, |f_{0020}|^2) \end{array} \right. . \quad (23)$$

### D. TBT analysis: Eq. (13) Vs Eq. (15)

Eq. (23) shows that the error of Eq. (13) is proportional to the calibration error  $\mathcal{E}$  and to square of the RDTs  $|f|^2$ . Since the latter are, to the first order, linearly dependent on the focusing errors, the error of Eq. (13) scales with  $\delta K_1^2$ , whereas the uncertainty of Eq. (15) scales with  $\delta K_1$ , as indicated by Eq. (20). From a purely theoretical point of view, hence, either formula is to be preferred to the other according to the largest source of uncertainty. If BPM calibration errors  $\mathcal{E}$  are either unknown or expected to be larger than  $\bar{h}_{ij}$  of Eq. (19) (i.e. of the focusing errors between three BPMs), beta functions are better inferred by Eq. (15). If the opposite is true, then Eq. (13) is to be preferred.

As far as the ESRF storage ring is concerned, BPM calibration factors are routinely fitted from the analysis of measured ORM. In the top plot of Fig. 2 the mean values over 32 measurement repeated during one whole year of operation are displayed along with the error bars representing their standard deviation. The rms (systematic) BPM gain error is of about 0.7% (2.7% maximum), with rms (random) error bars below 0.1%. It is worthwhile noticing that these calibrations factors refers to Libera BPMs operating in slow (orbit) acquisition mode and that they may vary in the fast (TBT) acquisition mode. In the bottom plot of Fig. 2 the variation of the RDT amplitudes along the ring is showed for the same lattice error of Fig. 1. With  $\langle |f_{2000}| \rangle$  of about 0.9% (2.1% maximum), which is larger than  $\langle |f_{0020}| \rangle$ , the RDT-related rms uncertainty  $64|f|^2$  of Eq. (22) is then of about 0.6% (2.8% maximum).

The bottom plot of Fig. 1 shows the error of Eq. (15) associated to  $\delta K_1$  via the  $\bar{h}_{ij}$ : 0.25% rms (2.1% peak-to-peak). Even admitting that the BPM calibration factors of Fig. 2 are applicable to TBT data and can be used in Eq. (13), this formula is expected in any case to be less precise (residual rms error of 0.6%) than Eq. (15) (residual rms error of 0.25%). For storage rings with lower rms beta beating (which is of about 5% at the ESRF) the opposite might be true.

The above considerations are rather mathematical and other aspects are to be taken into account when selecting the best approach for the evaluation of the beta function. First, Eq. (15) relies on the perfect synchronization between all BPMs, i.e. BPM reporting on the same turn and on the same bunch. Any systematic delay or jitter (even of a tiny fraction of revolution frequency) between the BPM data acquisition, would result in an arti-

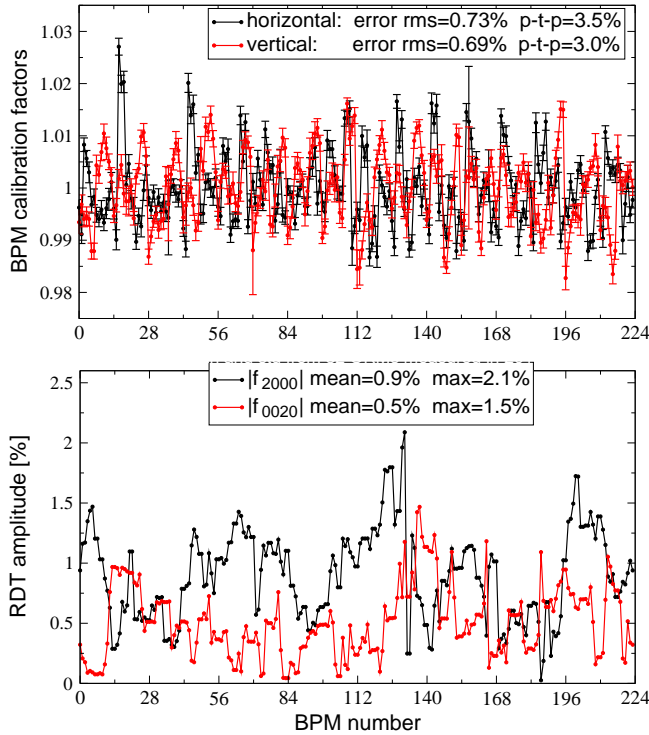


FIG. 2. (Color) Top: ESRF’s effective BPM calibration factors  $C_{x,y}$  inferred from the analysis of the orbit response matrix, averaged over 32 measurements repeated during one whole year of operation. The error bars represent their standard deviation. Bottom : variation of the focusing RDT amplitudes along the ESRF storage ring for the same lattice error of Fig. 1.

ficial BPM phase advance error, since the initial arbitrary phase  $\psi_0$  of Eq. (10) would be no longer the same for all BPMs and, hence, not canceled out in Eq. (14).

$$\Delta\Phi_{ij} = \Delta\phi_{ij} + \delta\phi_{ij}^{(tim)} \quad , \quad (24)$$

where  $\delta\phi_{ij}^{(tim)}$  is the phase error introduced by the monitors relative delay. The BPMs in the ESRF storage ring, for instance, are synchronized within about  $0.1 \mu\text{s}$  (peak-to-peak) over a revolution time of  $2.82 \mu\text{s}$ . Eq. (13) does not suffer from such a constraint and would work even with BPMs reporting on different turns. Second, the presence of trigonometric functions in the denominator of Eq. (14) requires that BPMs are separated by a phase advance away from either zero or multiples of  $\pi$ , to prevent the cotangent from becoming infinite. If this is the case, the triplet can be defined by using BPMs further downstream, as indicated in Ref. [19]. This may come to the price of increasing the number of sources of focusing errors between the BPMs, i.e.  $\bar{h}_{ij}$ , and in turn the measurement error of Eq. (20). Eq. (13) is not affected by the relative position of the BPMs.

### E. ORM and TBT analysis: impact of BPM resolution and ultra-low coupling

Ideally, ORM and TBT should be generated by exciting the beam (with orbit correctors and dipole kickers, respectively) so to optimize the signal-to-noise ratio, while remaining in the linear regime of the betatron motion. In this section rough estimates of the beam excitation amplitudes ensuring sufficient resolution are provided for the ESRF storage ring equipped with commercial Libera *Brilliance* BPMs and operating with ultra-low coupling, i.e. with a ratio between the betatron equilibrium emittances  $E_x/E_y \simeq 1\%$ . The question whether these amplitudes remain in the linear regime or not is addressed in the next sections.

ORMs are measured by using the BPMs in the slow-mode acquisition (10 Hz), which ensures a resolution of about 10 nm. Specialists prefer to define the BPM resolution as *integrated noise spectrum* or *integrated rms noise* [32, 33], denoted as measured uncertainty for frequencies integrated from 0.1 Hz or 1 Hz up to a specified bandwidth and represented by a spatial resolution per square root of the bandwidth (the noise being typically expected to be white so that the measurement error would decrease with the square root of the bandwidth). For the Libera *Brilliance* BPMs, the typical value in slow-mode acquisition is  $10 \text{ nm}/\sqrt{\text{Hz}}$ . Since the resolution depends on the beam intensity too, ORM measurements are performed at 30 mA, which ensure sufficient beam signal while remaining low enough to prevent beam induced effects on the orbit motion. The rms orbit distortion is of 200-250  $\mu\text{m}$  in the plane of the steerer, 2-5  $\mu\text{m}$  in the other one because of the ultra-low coupling achieved in the machine. Despite this low orbit distortion in the orthogonal plane, data remain more than two orders of magnitude above the noise floor (10 nm), permitting a reliable coupling measurement.

TBT data are acquired by switching the BPMs into the  $\sim 355 \text{ kHz}$  acquisition mode, whose expected resolution is in the  $\mu\text{m}$  range. Two independent evaluations of the noise floor with beam (one recording TBT data of the unperturbed beam, the other via SVD of the BPM matrix) indicate that the actual noise floor is of about 10  $\mu\text{m}$ . This accounts also for the natural beam motion which can be corrected by a fast orbit correction scheme during operation but not during the acquisition of TBT data (the method requires free oscillations). The resolution of TBT data is then three orders of magnitude worse than in the ORM measurement. This has a dramatic consequence in the minimum beam excitation necessary for a robust evaluation of coupling via TBT data. This is performed by analyzing the coupling lines of the TBT spectrum,  $H(0,1)$  and  $V(1,0)$  of Eq. (16),

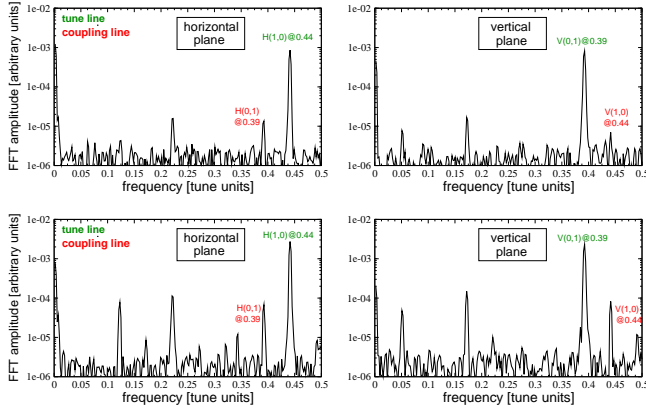


FIG. 3. (Color) Examples of spectra from measured TBT BPM data of the ESRF storage ring. Because of the ultra-low coupling, data with an initial excitation of 1 mm ( $\beta_x = 35$  m) and 0.3 mm ( $\beta_x = 3$  m) result in coupling lines close to the background noise (top plots). In order to limit the latter to about 2% of the coupling lines, the initial oscillations need to be tripled (bottom plots).

whose amplitudes in real units [m] read

$$\begin{cases} |H(0,1)|_{[m]} = 2\sqrt{\frac{\beta_x}{\beta_y}} \times |V(0,1)|_{[m]} \times |F_{xy}| \\ |V(1,0)|_{[m]} = 2\sqrt{\frac{\beta_y}{\beta_x}} \times |H(1,0)|_{[m]} \times |F_{yx}| \end{cases}. \quad (25)$$

The beta functions at the BPMs are such that both square roots in the above expressions range between 0.4 and 2.8:  $\sqrt{\beta_{x,y}/\beta_{y,x}} \sim 1$  can be then assumed. Because of the ultra-low coupling, the amplitudes of combined RDTs  $|F|$  are of the order of  $10^{-2}$ . An excitation in both planes of 1 mm ( $|H(1,0)|_{[m]} \sim |V(0,1)|_{[m]} \sim 10^{-3}$  m, since these are by far the largest harmonics of the TBT signal) would result then in coupling lines  $|H(0,1)|_{[m]} \sim |V(1,0)|_{[m]} \sim 10 \mu\text{m}$ , which is of the same order of magnitude than the noise floor (see upper plots of Fig. 3).

In conclusion, even though a tune line of  $\sim 1$  mm would suffice for a reliable analysis of focusing errors, the evaluation of ultra-low coupling via the secondary harmonics would be rather inaccurate. Hence, unless the BPM resolution in TBT mode and the natural beam stability are significantly improved, an initial oscillation of several mm is necessary for a robust and complete study of the linear lattice errors with TBT data (see lower plots of Fig. 3). These numbers may of course be different in other 3rd generation (and more recent) light sources, but the orders of magnitude are expected to be similar as long as they operate with ultra-low coupling and comparable BPM spectral background noise.

## F. TBT analysis: Can higher-order terms may be really neglected?

The harmonic analysis of TBT data discussed here, as well as other techniques analyzing the BPM matrix, assumes that the tune line (or the *betatron mode*) is exclusively generated by quadrupolar terms, independent of the initial oscillation amplitude.

In Appendix B more general expressions for the tune line amplitude and BPM phase advance in the nonlinear (amplitude dependent) regime are derived. The result is

$$\begin{cases} \Delta\Phi_{H,ij} = \Delta\phi_{x,ij}^{(mod)} + \arg\{B_{x,i} - B_{x,j}\} - 2h_{1100,ij} \\ \quad - 4h_{2200,ij}(2I_x) - 2h_{1111,ij}(2I_y) \\ \Delta\Phi_{V,ij} = \Delta\phi_{y,ij}^{(mod)} + \arg\{B_{y,i} - B_{y,j}\} - 2h_{0011,ij} \\ \quad - 2h_{1111,ij}(2I_x) - 4h_{0022,ij}(2I_y) \\ |H(1,0)_j| = \frac{\sqrt{2I_x}}{2} |B_{x,j}| \\ |V(0,1)_j| = \frac{\sqrt{2I_y}}{2} |B_{y,j}| \\ \begin{cases} B_{x,j} = 1 + i4f_{2000,j}^* + iF_{xx,j}(K_2^2, K_3, I_{x,y}) + T_{H,j}(K_2^2, I_{x,y}) \\ B_{y,j} = 1 + 4if_{0020,j}^* + iF_{yy,j}(K_2^2, K_3, I_{x,y}) + T_{V,j}(K_2^2, I_{x,y}) \end{cases} \end{cases}, \quad (26)$$

The functions  $F$  and the octupolar-like amplitude dependent detuning terms  $h$  are proportional to octupolar fields ( $\propto K_3$ ) and to quadratic functions of sextupole strengths ( $\propto K_2^2$ ), whereas  $T$  scales quadratically with  $K_2$ .

The above expressions indicate that when the initial oscillation amplitude ( $2I$ ) is *too large*, the betatron BPM phase advance  $\Delta\phi_{ij}$  is no longer measurable from the difference of the tune line phases  $\Delta\Phi_{ij}$ , since (octupolar-like) amplitude dependent focusing terms *corrupt* the tune line. The same is true for the invariant itself ( $2I$ ), which is no longer measurable from the tune line amplitude. In fact, the latter is not anymore constant along the ring and its modulation depends on the invariant itself via the functions  $F$  and  $T$  of Eq. (26).

There are two ways to estimate the maximum acceptable initial oscillation preventing nonlinearities from polluting the linear analysis of the tune line. The first is to evaluate the explicit expressions for  $B$  and  $h$  from the nonlinear lattice model. The second is to perform the harmonic analysis of single-particle tracking. To this end, it is enough to compare the tune line modulation and the deviation of the BPM phase advance  $\Delta\Phi_{ij}$  from the betatron phase  $\Delta\phi_{ij}$  for an ideal model with no focusing error. By repeating this test for several initial conditions, a threshold can be set to ensure a certain limit to the pollution. In Fig. 4 the results of four different tests are reported for the horizontal tune line. The impact on the vertical tune line is weaker because of the stronger horizontal focusing and chromaticity which result in a stronger impact of nonlinearities in that plane. A single particle has been tracked through the ideal lattice (i.e. with no focusing error,  $f_{2000} = f_{0020} = 0$  along the ring)



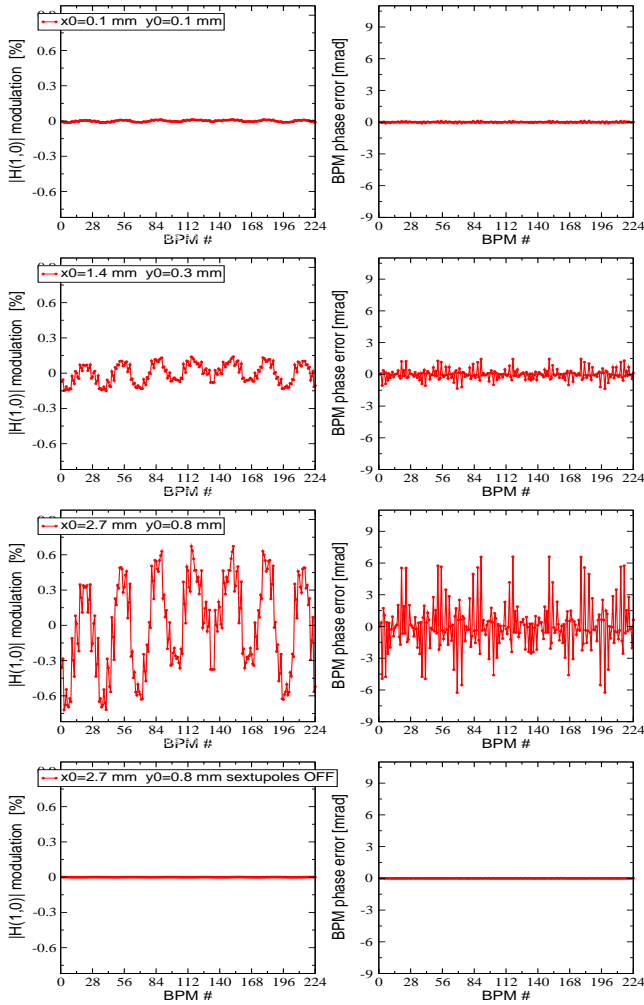


FIG. 4. (Color) Modulation of the horizontal tune line amplitude (left) and error of the BPM phase advance  $\Delta\Phi_{x,ij}$  inferred from the tune line phase with respect to the betatron BPM phase advance  $\Delta\phi_{x,ij}$  (right) obtained from single particle tracking simulations with different initial conditions. The large BPM phase error observed at  $(x_0, y_0) = (2.7, 0.8)$  mm (third row) disappears when nonlinear magnets are removed from the lattice model of the ESRF storage ring (last row). For the vertical tune line (not shown) amplitude modulation and phase errors are about a factor two and three lower, respectively.

of the ESRF storage ring for 1024 turns. The positions recorded at the 224 BPMs are Fourier analyzed and the tune line amplitude is used to evaluate the modulation of  $|H(1,0)|$  (left plots) along the ring due to the nonlinear terms  $F$  and  $T$  of Eq. (26). The tune line phase is used to compute the BPM phase advance  $\Delta\Phi_{ij}$  and its difference with the betatron phase advance  $\Delta\phi_{ij}$  is reported in the right plots. The test is first run for an extremely low initial excitation of  $100 \mu\text{m}$  in both planes (uppermost plot), then  $(x_0, y_0) = (1.4, 0.3)$  mm (second plot) and  $(x_0, y_0) = (2.7, 0.8)$  mm (third plot). Even though the tune line modulation is relatively modest, below 0.3% rms, a sizable deviation from the betatron phase ad-

vance of 2.6 mrad rms (6.6 mrad maximum), roughly corresponding to an rms *artificial* beta beating of 1%, is observed in the last case  $((x_0, y_0) = (2.7, 0.8)$  mm). This means that the linear analysis carried out in Ref. [23], which fitted quadrupolar errors from similar TBT data to best match  $\Delta\phi_{ij}$  and  $\Delta\Phi_{ij}$  up to 0.9 mrad rms, was indeed erroneous, since a great part of the initial deviation came from the nonlinear terms of Eq. (26) and not from quadrupolar errors. The confirmation that such deviations from the betatron parameters stem from nonlinear magnets is given in the lower most plot, where both the invariant and the betatron phase advance are retrieved with the same initial conditions  $(x_0, y_0) = (2.7, 0.8)$  mm after turning off all sextupoles and octupoles in the lattice model.

The results of Fig. 4 have important consequences on the possibility of using TBT data for a complete linear analysis of the ESRF storage ring. The above simulations indeed suggest to limit the initial oscillation amplitude to about 1.4 mm horizontally and 0.3 mm vertically in order to limit the nonlinear contribution to the BPM phase to less than 0.5 mrad rms. On the other hand, in Sec. III E it was shown that at this level of excitation the coupling analysis via the spectral lines  $H(0,1)$  and  $V(1,0)$  becomes inaccurate when the machine operates (as it has been doing since 2010) with ultra-low coupling.

### G. TBT analysis: which model BPM phase advance?

A possible way out to this dilemma can be found in replacing as reference betatron phase advance the one computed from the lattice  $\Delta\phi_{ij}$  (`ptc_twiss` command in MADX or `linopt` function in AT) with the BPM phase advance  $\Delta\Phi_{ij}^{(SPT)}$  inferred from the harmonic analysis of single-particle tracking simulations with the same oscillation amplitudes of the measured data. The linear analysis could be then performed on the difference between measured and model BPM phase advances, namely

$$\delta\Delta\phi_{ij}(\delta K_1) \simeq \Delta\Phi_{ij}^{(meas)}(\delta K_1, K_2, K_3, I_{x,y}) - \Delta\Phi_{ij}^{(SPT)}(K_2, K_3, I_{x,y}), \quad (27)$$

since in first approximation (i.e. by ignoring sextupole and octupole errors) the amplitude dependent nonlinear terms  $B$  and  $h_{pprr}$  of Eq. (26) would cancel out and the difference would depend on quadrupole errors only via  $\delta\Delta\phi_{ij}$ .

By doing so, however, the quality of the linear analysis would become dependent on the nonlinear lattice setting and model, as well as on tracking parameters, since they all affect  $\Delta\Phi_{ij}^{(SPT)}$ . In Fig. 5 the results of three numerical tests are reported for the same (linear and nonlinear) optics of Fig. 1. The center plot shows how actually the inclusion of nonlinear magnetic errors in the model does indeed influence  $\Delta\Phi_{ij}^{(SPT)}$ . A weak dependence on the

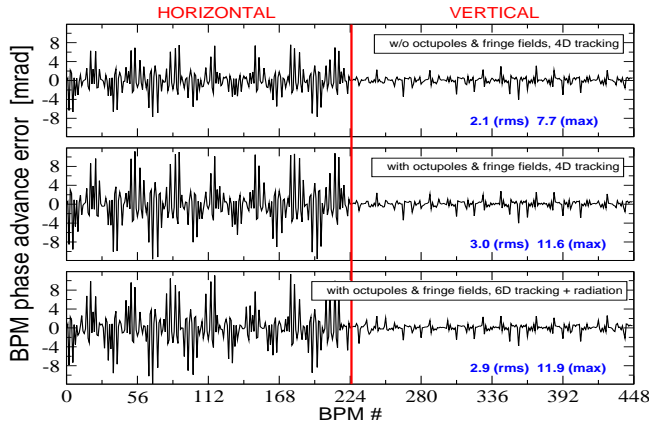


FIG. 5. (Color) BPM phase advance error  $\Delta\Phi_{ij}^{(SPT)} - \Delta\phi_{ij}$  evaluated from single-particle simulations with initial conditions  $(x_0, y_0) = (2.7, 0.8)$  mm against tracking parameters and additional nonlinearities on top of the sextupoles: 4D tracking with ideal sextupole setting (top), including the same nonlinear lattice error model (sextupole errors, octupolar field component in quadrupoles and fringe fields) of Ref. [23] (center), and 6D tracking including radiation effects (bottom).

inclusion of longitudinal tracking with radiation effects can be also observed in the lower most plot.

It can be argued that the beam itself is not a single particle and that its multi-particle nature and its finite rms emittances ( $E_x = 4$  nm,  $E_y = 4$  pm,  $\sigma_p = 0.1\%$  for the ESRF electron beam) would require an even more realistic approach to account for the damping of the TBT signal of its centroid (i.e. decoherence) due to chromaticity, amplitude dependent detuning [34–36] and possibly radiation effects. To this end, multi-particle tracking simulations and the harmonic analysis on the TBT motion of the beam centroid could be performed to infer the corresponding BPM phase advance  $\Delta\Phi_{ij}^{(MPT)}$ .

In the top plots of Fig. 6 the simulated TBT signal at one BPM is shown for three different sextupole settings of the ESRF storage ring: with low chromaticity and detuning with amplitude (*special optics*, typically used for TBT studies), with low chromaticity but large detuning (*multi-bunch optics*), and high vertical chromaticity and low detuning (*few-bunch optics*). Tracking is performed in the transverse plane only (4D) with frozen longitudinal motion and no radiation effects. The decoherence is much more visible in the horizontal plane because of the much larger horizontal emittance compared to the vertical plane. Simulations were run with no betatron coupling. In the bottom plots of Fig. 6 the BPM phase difference between multi-particle and single-particle BPM phase advance,  $\Delta\Phi_{ij}^{(MPT)} - \Delta\phi_{ij}^{(SPT)}$ , is plotted along the ring: Deviations are more pronounced in the horizontal plane (as expected from the stronger decoherence) though they are a mere 10% of  $\Delta\phi_{ij}^{(SPT)}$  of Fig. 5.

Since the spectral resolution of the harmonic analysis depends on the number of turns suitable to be Fourier-analyzed, the quality of the linear analysis is expected

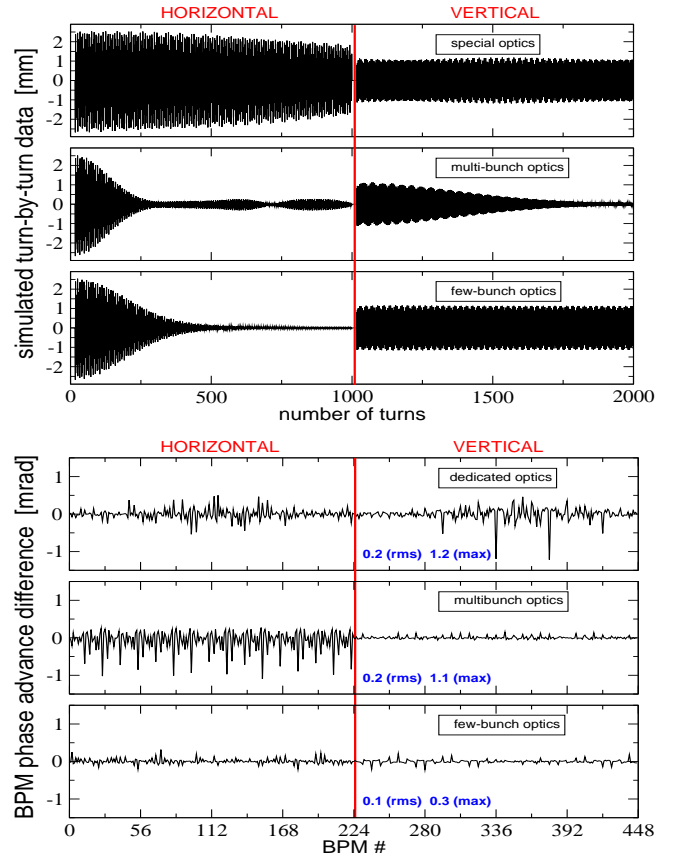


FIG. 6. (Color) Top: TBT beam centroid oscillation obtained from multi-particle 4D tracking (Gaussian distribution,  $5 \times 10^4$  particles,  $E_x = 4$  nm,  $E_y = 4$  pm,  $\sigma_p = 0.1\%$ ). Three various sextupole settings of the ESRF storage ring are tested: low chromaticity and weak detuning with amplitude (*special optics*), low chromaticity and strong detuning (*multi-bunch optics*), and high vertical chromaticity and weak detuning (*few-bunch optics*). Bottom: corresponding BPM phase advance deviation between the harmonic analysis of a multi-particle TBT signals with respect its single-particle counterpart,  $\Delta\Phi_{ij}^{(MPT)} - \Delta\phi_{ij}^{(SPT)}$ .

to increase with the number of turns. This effect is displayed in Fig. 7, where the difference  $\Delta\Phi_{ij}^{(MPT)} - \Delta\phi_{ij}^{(SPT)}$  is showed for two different nonlinear optics against the number of turns used for the FFT. Differently from Fig. 6, tracking is here performed in all planes (6D) including radiation effects. In both cases, when 512 or more turns are analyzed multi-particle effects appear to account for a mere fraction of mrad.

These and other multi-particle simulations confirm that the multi-particle effects are negligible compared to  $\Delta\phi_{ij}^{(SPT)}$  and that the latter can be effectively used for a linear analysis via Eq. (27), provided that a solid nonlinear lattice model is available.

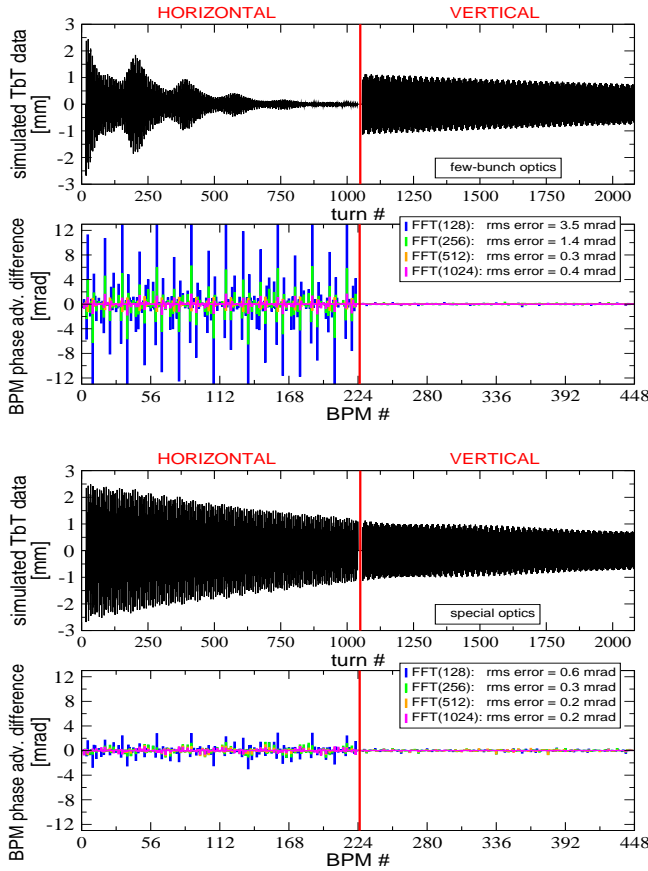


FIG. 7. (Color) BPM phase advance error  $\Delta\phi_{ij}^{(MPT)} - \Delta\phi_{ij}^{(SPT)}$  evaluated against the number of turns used in the harmonic analysis for two different sextupole settings, with strong decoherence (top) and negligible attenuation (bottom). The same multi-particle simulations of Fig. 6 is used, this time with a full 6D tracking including radiation effects.

#### H. TBT analysis: Can beta beating and ultra-low coupling be evaluated with separate measurements?

It can be argued that TBT analysis of focusing errors and betatron coupling at the ESRF storage ring could be carried out with two separate measurements: one at low excitation amplitude for the evaluation and correction of beta beating only (with no or limited *pollution* of the tune lines by nonlinear terms), and a second with large oscillation to enhance the coupling spectral lines well above the noise floor. While the first measurement is perfectly feasible, two main obstacles prevent the second from being viable.

First, at large amplitudes nonlinear terms affect the coupling spectral lines too. In Appendix C analytic expressions for the coupling lines of the real signals  $\tilde{x}$  and  $\tilde{y}$  including the leading amplitude dependent terms are

derived:

$$\begin{cases} |H(0,1)_j| = |F_{xy,j}(J_1) + T_{xy,j}(J_3, K_3, K_2^2, J_1, I_{x,y})| \sqrt{2I_y} \\ |V(1,0)_j| = |F_{yx,j}(J_1) + T_{yx,j}(J_3, K_3, K_2^2, J_1, I_{x,y})| \sqrt{2I_x} \\ \arg\{H(0,1)_j\} = \phi_{x,j} + \psi_{x0} + \arg\{F_{xy,j} + T_{xy,j}\} - \frac{\pi}{2} \\ \arg\{V(1,0)_j\} = \phi_{y,j} + \psi_{y0} + \arg\{F_{yx,j} + T_{yx,j}\} - \frac{\pi}{2} \end{cases}, \quad (28)$$

where the betatron coupling terms  $F_{xy}$  and  $F_{yx}$  are the same of Eq. (16). The complex nonlinear amplitude dependent coupling functions  $T_{xy}$  and  $T_{yx}$ , defined in Eq. (C2), scale linearly with the skew octupole gradient  $J_3$ , as well as with the products  $K_3J_1$  (cross product between normal octupole and skew quadrupole strengths) and  $K_2^2J_1$  (cross product between normal sextupole and skew quadrupole fields). Hence, even in the absence of physical octupoles, normal sextupoles excite  $T_{xy}$  and  $T_{yx}$  via betatron coupling. Since both  $F_{xy}$  and  $F_{yx}$  scale linearly with  $J_1$  too, the overall amplitude dependent modulation of the coupling lines scales quadratically with the sextupole fields, i.e. with the same order of magnitude of the tune line modulation  $B_{x,y}$  and  $h_{pprr}$  of Eq. (26). The analysis of the coupling lines to evaluate betatron coupling at large amplitudes would then be corrupted by the machine nonlinearities in the same way the study of focusing errors from the tune lines would be.

Second, the tune lines are used to extract the coupling RDTs  $f_{1001}$  and  $f_{1010}$  (or their combined functions  $F_{xy}$  and  $F_{yx}$ ) via Eqs. (16)-(17). If a large excitation is imparted to generate measurable coupling lines, the nonlinear terms contributing to the tune line amplitudes and phase,  $B_{x,y}$  of Eq. (26), would corrupt the evaluation of the coupling RDTs, since  $|H(1,0)| \neq \sqrt{2I_x}$ ,  $|V(0,1)| \neq \sqrt{2I_y}$ ,  $\arg\{H(1,0)\} \neq \phi_x + \psi_{x0}$  and  $\arg\{V(0,1)\} \neq \phi_y + \psi_{y0}$ .

An example of betatron coupling analysis corrupted by nonlinear terms is shown in Fig. 8. The harmonic decomposition is carried out on simulated single-particle TBT BPM data with the lattice of the ESRF storage ring comprising 64 skew quadrupoles distributed along the ring, whose normalized integrated strengths  $J_1$  are reported in the upper plot. By assuming that the coupling lines  $H(0,1)$  and  $V(1,0)$  are generated only by betatron coupling terms  $F_{xy}$  and  $F_{yx}$ , respectively, the latter are inferred and used to extract the strengths of the 64 skew quadrupoles by pseudo-inverting the system of Eqs. (16) and (9). This exercise has been repeated for three different sextupoles settings and at diverse initial excitations. The errors remain in the few percent level when the initial displacement is of about 1 mm (center plot), though this amplitude is too low for real measurements. However, when simulating oscillation amplitudes sufficient to generate measurable coupling spectral lines, the rms error ranges from 25% to 100% depending on the nonlinear setting (bottom plot). When turning off all sextupoles in the lattice (along with any other nonlinearities) the rms error remains well below 0.5% for any initial condition.

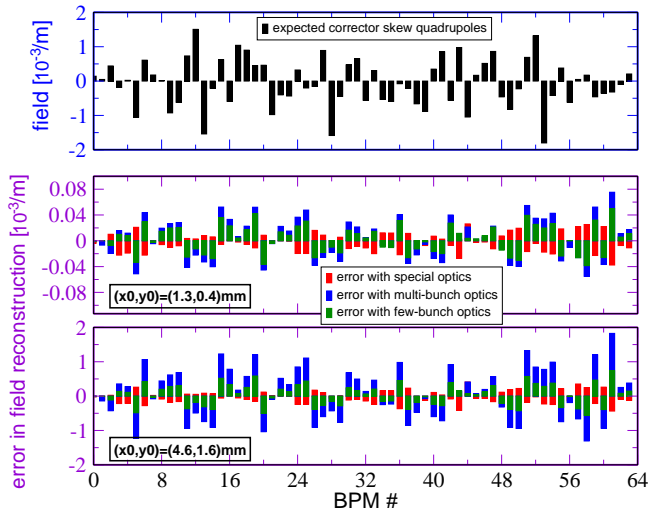


FIG. 8. (Color) Example of simulated betatron coupling analysis corrupted by nonlinear terms. The coupling lines  $H(0,1)$  and  $V(1,0)$  of simulated single-particle TBT BPM data with the lattice of the ESRF storage ring comprising 64 skew quadrupoles (top plot) are assumed to be excited by linear coupling functions  $F_{xy}$  and  $F_{yx}$  only. They are inferred via Eq. (16) and the skew quadrupole strengths retrieved by pseudo-inverting the system via Eq. (9). At low amplitude the difference between set and reconstructed skew quadrupole fields is of a few percent (center plot), while at large initial excitation it increases to 25% and 100% depending on the sextupole settings (bottom plot). When sextupoles are turned off in the model (which does not comprise octupoles), the errors remains well below 0.5% (not shown), irrespective of the initial conditions.

#### IV. CONCLUSION

Analytic formulas for the evaluation of linear lattice parameters from either turn-by-turn beam position data or an error lattice model have been derived and used to perform an error analysis. This study also presented a procedure for the estimation of detrimental effects of nonlinear terms stemming from sextupoles and higher order multipole magnets. These may result in a wrong evaluation of the BPM phase advance and hence of the focusing errors. Preliminary single-particle simulations however would suffice to properly account for such nonlinear terms. It has been also shown how beam decoherence does not corrupt the evaluation of the BPM phase advance, the error found in multi-particle simulations being the same determined by single-particle tracking (within a 10% uncertainty).

The elements presented in this paper indicate that for the ESRF electron storage ring operating with ultra-low coupling and making use of the Libera *Brilliance* BPMs, the analysis of the linear lattice errors (focusing and coupling) is limited in its accuracy and precision by several factors. As a rule of thumb, 3 mrad of rms BPM phase advance error correspond to about 1% of rms beta beating. The ORM analysis is to be preferred to the harmonic study of TBT data for several reasons:

- The ORM analysis of focusing errors and coupling requires a maximum beam excitation of about  $250 \mu\text{m}$  well within the linear regime of the betatron motion.
- Because of the natural beam motion (vibrations), the worse BPM resolution when operating in TBT mode and the need of measuring an ultra-low coupling, the harmonic analysis requires a minimum beam excitation of some mm, reaching a region of the betatron motion where magnetic nonlinearities reduce the measurement accuracy in the range of 2-6 mrad for the rms BPM phase advance error and of 1% – 2% in the evaluation of the beta beating (depending on the sextupole settings). If nonlinear terms are not taken into account, the inferred quadrupolar errors would wrongly account for sextupolar and octupolar contributions to the betatron motion.
- Formulas for the evaluation of beta beating from TBT data are affected by intrinsic errors at the level of  $\sim 0.3\%$  rms ( $\sim 2\%$  peak to peak) if the BPM phase advance is used (and a perfect synchronization between the monitors is assumed), whereas if the tune line amplitude is used (and BPM calibration factors inferred from orbit data can be trusted) the uncertainty is of  $\sim 0.6\%$  rms ( $\sim 3\%$  maximum). No error estimate for the ORM analysis has been performed so far.

The above numbers may clearly vary in other ring-based light sources, though recent comparisons between ORM and TBT analysis of linear lattice errors in other facilities report similar uncertainties [12, 13].

The same considerations made here for the FFT-based analysis of TBT data should apply the techniques of Refs. [10, 11, 26–28]. Indeed the nonlinearities of Eq. (26) affecting the tune lines are expected to alter the *betatron modes* which are used for the evaluation of focusing errors. In these schemes, in fact, it is assumed that any deviation from the ideal betatron modes, i.e. those oscillating at the frequency of the linear tunes, would stem from quadrupolar errors, whereas Eq. (26) suggests that at *large* amplitudes (needed for the analysis of ultra-low coupling) the impact of nonlinear effects needs to be assessed. Hence, as for the harmonic analysis, if nonlinearities are ignored, the inferred quadrupolar errors would wrongly account for sextupolar and octupolar contributions to the betatron motion.

A last consideration worth to be made concerns the new ESRF storage ring under design (and possibly any new light source with sub-nm natural horizontal emittance). The new lattice design is expected to provide a natural emittance of about 130 pm (4 nm today) and features beta functions globally much smaller than in the existing machine. Today the lowest beta function at the BPMs is of about 5.6 m. In the new machine two BPMs (out of ten) per cell are located in regions with  $\beta_x = 1.1$



m ( $\beta_y = 3.3$  m), and  $\beta_x = 1.9$  m ( $\beta_y = 2.3$  m) in other two monitors. In the future storage ring the BPM electronics remains based on the existing Libera *Brilliance* hardware (additional Libera *Spark* modules will be installed to cover the increased number of monitors). This means that in order to preserve today's spectral resolution, the initial beam excitation, i.e. the invariant, shall be larger by about a factor two, in a machine which is by far more nonlinear than the existing one. This casts even stronger concerns on the possibility of measuring and correcting linear optics (focusing errors and betatron coupling) via TBT data in the upcoming storage

ring.

The above conclusions are expected not to apply to hadron circular accelerators with less aggressive focusing lattices and larger regions of the betatron phase space, i.e. the invariants, within the linear optics regime.

## V. ACKNOWLEDGMENT

I am deeply indebted with Rogelio Tomás for inspiring this work. I am also grateful to him and Reine Versteegen for reading the original manuscript and for providing precious comments and suggestions during its preparation.

### Appendix A: Linear lattice parameters with focusing errors

In Appendix C of Ref. [23] a non-truncated expression for the tune lines  $H(1, 0)$  and  $V(0, 1)$  is derived assuming ultra low coupling, i.e. that coupling RDTs are negligible compared to the ones excited by focusing errors,  $f_{2000}$  and  $f_{0020}$ . A second, though not less important, assumption is that the impact on the tune lines from nonlinear RDTs is negligible, i.e. that the oscillation amplitudes ( $2I_{x,y}$ ) are low enough to prevent octupolar-like RDT  $f_{3100}$ ,  $f_{2011}$ ,  $f_{0031}$  and  $f_{1120}$  from contributing to  $H(1, 0)$  and  $V(0, 1)$ , See Table V-VII of Ref. [30]. Note that the spectral lines reported there refer to the complex signals  $h_x = \tilde{x} - i\tilde{p}_x$  and  $h_y = \tilde{y} - i\tilde{p}_y$ , for which the above octupolar-like RDTs excite the lines  $H_h(-1, 0)$  and  $V_h(0, -1)$ , hence introducing amplitude-dependent focusing errors. Since the harmonic analysis is performed here on the real signals  $\tilde{x}$  and  $\tilde{y}$ , those lines *pollute* the tune peaks, since  $H(1, 0) = 1/2[H_h(1, 0) + H_h^*(-1, 0)]$  and  $V(0, 1) = 1/2[V_h(0, 1) + V_h^*(0, -1)]$ . A more detailed discussion is made in the Appendices C and D of Ref. [23]. A third condition is that Hamiltonian octupolar-like terms  $h_{2200}(2I_x)^2$ ,  $h_{1111}(2I_x)(2I_y)$  and  $h_{0022}(2I_y)^2$  can be neglected, as they would introduce amplitude-dependent detuning and shifts of the betatron phase unrelated to linear lattice errors. It is worthwhile reminding that such nonlinear resonant and detuning terms are generated by octupole magnets (to the first order) as well as by sextupoles (to the second order) and are in general much stronger in light sources than in hadron machines (because of the higher natural chromaticity). Unless specified, throughout this appendix only ideal BPMs with calibration factors  $\mathcal{C}_{x,y} = 1$  are considered. Under these three important assumptions the tune lines at a generic BPM  $j$  read

$$\begin{cases} H(1, 0)_j = \frac{1}{2} \left[ \cosh(4|f_{2000,j}|) + i \sinh(4|f_{2000,j}|) e^{-iq_{2000,j}} \right] \sqrt{2I_x} e^{i(2\pi N Q_x + \phi_{x,j}^{(mod)} + \psi_{x0})} \\ V(0, 1)_j = \frac{1}{2} \left[ \cosh(4|f_{0020,j}|) + i \sinh(4|f_{0020,j}|) e^{-iq_{0020,j}} \right] \sqrt{2I_y} e^{i(2\pi N Q_y + \phi_{y,j}^{(mod)} + \psi_{y0})} \end{cases}, \quad (\text{A1})$$

where

$$\begin{cases} f_{2000,j} = \frac{\sum^W \beta_{x,w}^{(mod)} \delta K_{w,1} e^{2i\Delta\phi_{x,wj}^{(mod)}}}{8(1 - e^{4\pi i Q_x})} + O(\delta K_1^2) \\ q_{2000,j} = \arg \{ f_{2000,j} \} \end{cases}, \quad \begin{cases} f_{0020,j} = -\frac{\sum^W \beta_{y,w}^{(mod)} \delta K_{w,1} e^{2i\Delta\phi_{y,wj}^{(mod)}}}{8(1 - e^{4\pi i Q_y})} + O(\delta K_1^2) \\ q_{0020,j} = \arg \{ f_{0020,j} \} \end{cases}, \quad (\text{A2})$$

with  $\beta^{(mod)}$  and  $\Delta\phi^{(mod)}$  are the Courant-Snyder (C-S) parameters of the ideal lattice (i.e. without focusing errors  $\delta K_{w,1}$ ).  $O(\delta K_1^2)$  denotes the remainder proportional to the square of the focusing errors. The above sums run over all  $W$  quadrupole errors along the ring, and  $\Delta\phi_{wj}$  denotes the phase advance between the magnet  $w$  and the BPM  $j$ . Eq. (A1) may be rewritten as

$$H(1, 0)_j = \frac{1}{2} \sqrt{2I_x} A_{f,j} e^{i(2\pi N Q_x + \phi_{x,j}^{(mod)} + \theta_{f,j})}, \quad (\text{A3})$$

$$A_{f,j} = \left( 1 + 2 \sinh(4|f_{2000,j}|) \left[ \sinh(4|f_{2000,j}|) + \cosh(4|f_{2000,j}|) \sin q_{2000,j} \right] \right)^{1/2}, \quad (\text{A4})$$

$$\theta_{f,j} = \tan^{-1} \left\{ \frac{\sinh(4|f_{2000,j}|) \cos q_{2000,j}}{\cosh(4|f_{2000,j}|) + \sinh(4|f_{2000,j}|) \sin q_{2000,j}} \right\} + \psi_{x0}. \quad (\text{A5})$$

The  $s$ -dependent term  $A_f$  represents the phase space deformation induced by focusing errors not included in the model. With the ideal lattice the  $s$ -dependent phase space ellipses of the Cartesian coordinates are mapped into circles of constant radius  $\sqrt{2I_x}$  when moving in the C-S coordinates. With lattice errors not included in the model, the C-S transformation with the ideal C-S parameters will map the initial ellipses in other ellipses whose semi-axis depend on  $A_f$ . Only when those errors are included in the model  $f_{2000} = 0$  and  $A_f = 1$  along the ring, and the phase space circles are retrieved with the new C-S parameters and transformation.

**Analytic formulas for the beta beating:** By comparing Eq. (A3) and Eq. (11) (assuming an ideal BPM calibration factor,  $\mathcal{C} = 1$ ), the measured  $\beta$  can be interpreted as the initial model  $\beta^{(mod)}$  modified by the focusing errors via the RDTs so to have tune line amplitude constant along the ring and equal to  $\sqrt{2I}$ . This is equivalent to say that at the BPM  $j$   $\beta_{x,j} = \beta_{x,j}^{(mod)} A_{f,j}^2$ , i.e.

$$\begin{cases} \beta_{x,j} = \beta_{x,j}^{(mod)} \left\{ 1 + 2 \sinh(4|f_{2000,j}|) \left[ \sinh(4|f_{2000,j}|) + \cosh(4|f_{2000,j}|) \sin q_{2000,j} \right] \right\} \\ \beta_{y,j} = \beta_{y,j}^{(mod)} \left\{ 1 + 2 \sinh(4|f_{0020,j}|) \left[ \sinh(4|f_{0020,j}|) + \cosh(4|f_{0020,j}|) \sin q_{0020,j} \right] \right\} \end{cases}, \quad (\text{A6})$$

where the expression for the vertical plane follows from the same interpretation of  $V(0,1)$  in Eq. (A1). The beta beating then reads

$$\begin{cases} \frac{\Delta\beta_{x,j}}{\beta_{x,j}} = 2 \sinh(4|f_{2000,j}|) \left[ \sinh(4|f_{2000,j}|) + \cosh(4|f_{2000,j}|) \sin q_{2000,j} \right] \\ \frac{\Delta\beta_{y,j}}{\beta_{y,j}} = 2 \sinh(4|f_{0020,j}|) \left[ \sinh(4|f_{0020,j}|) + \cosh(4|f_{0020,j}|) \sin q_{0020,j} \right] \end{cases}. \quad (\text{A7})$$

To the first order in the RDTs the hyperbolic functions can be truncated to their leading terms,

$$\begin{cases} \beta_{x,j} = \beta_{x,j}^{(mod)} (1 + 8\Im\{f_{2000,j}\}) + O(|f_{2000}|^2) \\ \beta_{y,j} = \beta_{y,j}^{(mod)} (1 + 8\Im\{f_{0020,j}\}) + O(|f_{0020}|^2) \end{cases}, \quad \begin{cases} \left( \frac{\Delta\beta_x}{\beta_x} \right)_j = 8\Im\{f_{2000,j}\} + O(|f_{2000}|^2) \\ \left( \frac{\Delta\beta_y}{\beta_y} \right)_j = 8\Im\{f_{0020,j}\} + O(|f_{0020}|^2) \end{cases}. \quad (\text{A8})$$

$O(|f|^2)$  denotes the remainder proportional to the square of the RDT amplitude. To the first order in  $\delta K_1$  the RDTs can be substituted by Eq. (A2), yielding

$$\begin{cases} \left( \frac{\Delta\beta_x}{\beta_x} \right)_j^{(1)} \simeq + \frac{1}{2 \sin(2\pi Q_x)} \sum_w^W \beta_{x,w}^{(mod)} \delta K_{w,1} \cos(2|\Delta\phi_{x,wj}^{(mod)}| - 2\pi Q_x) \\ \left( \frac{\Delta\beta_y}{\beta_y} \right)_j^{(1)} \simeq - \frac{1}{2 \sin(2\pi Q_y)} \sum_w^W \beta_{y,w}^{(mod)} \delta K_{w,1} \cos(2|\Delta\phi_{y,wj}^{(mod)}| - 2\pi Q_y) \end{cases}, \quad (\text{A9})$$

which are the standard textbook formulas.

**Analytic formulas for the phase shift.** The phase space deformation introduced by  $A_f$  in Eq. (A3) and the resulting beta beating are accompanied by local jumps (or shifts) of the betatron phase with respect the ideal one. These are generated by the phase space deformation induced by the RDTs via the  $s$ -dependent term  $\theta_f$  in Eq. (A3) and by detuning Hamiltonian coefficient  $h_{1100}$  ( $h_{0011}$  in the vertical plane) which does not alter the phase space topology. The tune  $Q_x$  in Eq. (A3) is indeed equal to the ideal one minus the derivative of all additional phase-independent Hamiltonian terms,

$$Q_x = Q_x^{(mod)} - \frac{1}{2\pi} \frac{\partial \langle H \rangle_\phi}{\partial I_x} = Q_x^{(mod)} - \frac{1}{2\pi} \frac{\partial h_{1100}(2I_x)}{\partial I_x} + O(I_x) \simeq Q_x^{(mod)} - \frac{1}{\pi} h_{1100}, \quad (\text{A10})$$

$$h_{1100} = -\frac{1}{4} \sum_{w=1}^W \beta_{x,w}^{(mod)} \delta K_{w,1} + O(\delta K_1^2), \quad (\text{A11})$$

where the remainder  $O(I_x)$  includes amplitude-dependent octupolar-like detuning not discussed here, and  $O(\delta K_1^2)$  denotes the second order contribution to detuning from quadrupole errors (as well as from coupling) which is neglected

in the following derivation though it can be computed as shown in Ref. [23]. In the vertical plane the following relations apply

$$Q_y \simeq Q_y^{(mod)} - \frac{1}{\pi} h_{0011} \quad , \quad h_{0011} = +\frac{1}{4} \sum_{w=1}^W \beta_{y,w}^{(mod)} \delta K_{1,w} + O(\delta K_1^2) \quad . \quad (A12)$$

The betatron phase computed by any optics code refers always to the origin ( $s=0$ ). When comparing the betatron phases with and without lattice errors, it shall be noted that with errors the initial phase is not zero with respect to the ideal case, namely

$$\begin{cases} \phi_{x,s=0} = \theta_{f_{2000},s=0} \\ \phi_{x,j} = \phi_{x,j}^{(mod)} - 2h_{1100,j} + \theta_{f_{2000},j} - \phi_{x,s=0} \end{cases} \quad , \quad \begin{cases} \phi_{y,s=0} = \theta_{f_{0020},s=0} \\ \phi_{y,j} = \phi_{y,j}^{(mod)} - 2h_{0011,j} + \theta_{f_{0020},j} - \phi_{y,s=0} \end{cases} \quad . \quad (A13)$$

The  $s$ -dependent terms  $h_{1100,j}$  and  $h_{0011,j}$  include the focusing errors from the origin ( $s=0$ ) and the BPM  $j$ :

$$h_{1100,j} = -\frac{1}{2} \sum_{w=1}^{W<j} \beta_{x,w}^{(mod)} \delta K_{w,1} + O(\delta K_1^2) \quad , \quad h_{0011,j} = +\frac{1}{2} \sum_{w=1}^{W<j} \beta_{y,w}^{(mod)} \delta K_{w,1} + O(\delta K_1^2) \quad . \quad (A14)$$

Note that even if the final detuning is zero (in practice two or more dedicated quadrupole families are trimmed so to have the desired ideal tunes),  $h_{1100,j}$  and  $h_{0011,j}$  are in general nonzero along the ring. By manipulating Eq. (A13) the phase shift then reads

$$\begin{cases} \phi_{x,j} - \phi_{x,j}^{(mod)} = -2h_{1100,j} + \theta_{f_{2000},j} - \theta_{f_{2000},s=0} \\ \phi_{y,j} - \phi_{y,j}^{(mod)} = -2h_{0011,j} + \theta_{f_{0020},j} - \theta_{f_{0020},s=0} \end{cases} \quad . \quad (A15)$$

The truncation to the first order in the RDT of  $\theta_f$  from Eq. (A5) reads

$$\theta_{f_{2000},j} \simeq \tan^{-1} \left\{ \frac{4|f_{2000,j}| \cos q_{2000,j}}{1 + 4|f_{2000,j}| \sin q_{2000,j}} \right\} \simeq \tan^{-1} (4|f_{2000,j}| \cos q_{2000,j}) \simeq 4|f_{2000,j}| \cos q_{2000,j} \simeq 4\Re\{f_{2000,j}\} \quad (A16)$$

The equivalent approximation in the vertical plane yields to  $\theta_{f_{0020},j} \simeq 4\Re\{f_{0020,j}\}$ . Eq. (A15) then simplifies to

$$\begin{cases} \phi_{x,j} - \phi_{x,j}^{(mod)} = -2h_{1100,j} + 4\Re\{f_{2000,j} - f_{2000,s=0}\} + O(|f_{2000}|^2) \\ \phi_{y,j} - \phi_{y,j}^{(mod)} = -2h_{0011,j} + 4\Re\{f_{0020,j} - f_{0020,s=0}\} + O(|f_{0020}|^2) \end{cases} \quad . \quad (A17)$$

The shift of the BPM phase advance can be computed from the above expressions

$$\begin{cases} \Delta\phi_{x,ij} = \Delta\phi_{x,ij}^{(mod)} - 2h_{1100,ij} + 4\Re\{f_{2000,j} - f_{2000,i}\} + O(|f_{2000}|^2) \\ \Delta\phi_{y,ij} = \Delta\phi_{y,ij}^{(mod)} - 2h_{0011,ij} + 4\Re\{f_{0020,j} - f_{0020,i}\} + O(|f_{0020}|^2) \end{cases} \quad , \quad \begin{cases} h_{1100,ij} = -\frac{1}{2} \sum_{i<w<j} \beta_{x,w}^{(mod)} \delta K_{w,1} + O(\delta K_1^2) \\ h_{0011,ij} = +\frac{1}{2} \sum_{i<w<j} \beta_{y,w}^{(mod)} \delta K_{w,1} + O(\delta K_1^2) \end{cases} \quad , \quad (A18)$$

where the above sums extend over the focusing errors between the two BPMs  $i$  and  $j$  only. Since the latter monitor is downstream the former, i.e.  $s_j > s_i$ , the above sum is well defined. Explicit expressions truncated to the first order in  $\delta K_1$  similar to Eq. (A9) can be retrieved after substituting the RDTs in the above equations with Eq. (A2).

**Analytic formulas for the alpha shift.** The last C-S parameters to be evaluated is  $\alpha = -1/2\beta'$ , where the derivative is with respect to  $s$ . The beta function is the one of Eq. (A6). The derivative can be written as

$$\beta'(\beta^{(mod)}, |f|, q) = \frac{\partial\beta}{\partial\beta^{(mod)}} \beta'^{(mod)} + \frac{\partial\beta}{\partial|f|} |f|' + \frac{\partial\beta}{\partial q} q' \quad , \quad (A19)$$

Two approximations are made here to simplify the mathematical derivation. The first is that  $0 \simeq |f|' \ll \beta'^{(mod)}$ ,  $q'$  and corresponds to the fact that the variation along the ring of  $|f|$  can be neglected, this being much smaller than the one of oscillating functions  $\beta$  and  $q$ . The second is that  $q \simeq 2\phi^{(mod)}$ , see Eq. (A2). Both are actually exact conditions along regions free of focusing errors, as proved in Ref. [31]. From Eq. (A6) and the above relation,  $\alpha$  reads

$$\begin{aligned} \alpha_{x,j} \simeq & -\frac{1}{2} \beta_{x,j}'^{(mod)} \left\{ 1 + 2 \sinh(4|f_{2000,j}|) \left[ \sinh(4|f_{2000,j}|) + \cosh(4|f_{2000,j}|) \sin q_{2000,j} \right] \right\} \\ & - \beta_{x,j}^{(mod)} \sinh(4|f_{2000,j}|) \cosh(4|f_{2000,j}|) \cos q_{2000,j} q_{2000,j}' \quad . \end{aligned} \quad (A20)$$

Since  $q' \simeq (2\phi)' = 2/\beta^{(mod)}$  and  $\frac{1}{2}\beta^{(mod)} = \alpha^{(mod)}$ , the above expression becomes

$$\alpha_{x,j} \simeq \alpha_{x,j}^{(mod)} \left\{ 1 + 2 \sinh(4|f_{2000,j}|) \left[ \sinh(4|f_{2000,j}|) + \cosh(4|f_{2000,j}|) \sin q_{2000,j} \right] \right\} - \sinh(8|f_{2000,j}|) \cos q_{2000,j} \quad ,$$

and the alpha shifts  $\Delta\alpha = \alpha - \alpha^{(mod)}$  read

$$\begin{cases} \Delta\alpha_{x,j} \simeq \alpha_{x,j}^{(mod)} 2 \sinh(4|f_{2000,j}|) \left[ \sinh(4|f_{2000,j}|) + \cosh(4|f_{2000,j}|) \sin q_{2000,j} \right] - \sinh(8|f_{2000,j}|) \cos q_{2000,j} \\ \Delta\alpha_{y,j} \simeq \alpha_{y,j}^{(mod)} 2 \sinh(4|f_{0020,j}|) \left[ \sinh(4|f_{0020,j}|) + \cosh(4|f_{0020,j}|) \sin q_{0020,j} \right] - \sinh(8|f_{0020,j}|) \cos q_{0020,j} \end{cases} \quad . \quad (\text{A21})$$

By keeping only the leading terms from the hyperbolic functions, the following first-order expression is retrieved

$$\begin{cases} \alpha_{x,j} \simeq \alpha_{x,j}^{(mod)} (1 + 8\Im\{f_{2000,j}\}) - 8\Re\{f_{2000,j}\} + O(|f_{2000}|^2) \\ \alpha_{y,j} \simeq \alpha_{y,j}^{(mod)} (1 + 8\Im\{f_{0020,j}\}) - 8\Re\{f_{0020,j}\} + O(|f_{0020}|^2) \end{cases} \quad . \quad (\text{A22})$$

Explicit expressions truncated to the first order in  $\delta K_1$  similar to Eq. (A9) can be retrieved after substituting the RDTs in the above equations with Eq. (A2).

**Improved formula to evaluate the beta beating from BPM phase advance.** Eq. (15) was derived in Ref. [3] under the assumption that the region between the three BPMs is free of unknown focusing errors. Here a more general formula is derived, which does not requires this condition. The only approximation made is a series of truncations to the first order in  $\delta K_1$ , and hence in the RDTs  $f_{2000}$  and  $f_{0020}$ . The starting point are Eqs. (A8), (A18), (A22)

$$\begin{cases} \beta_j \simeq \beta_j^{(mod)} (1 + 8\Im\{f_j\}) \\ \Delta\phi_{ij} \simeq \Delta\phi_{ij}^{(mod)} - 2h_{ij} + 4\Re\{f_j - f_i\} \\ \alpha_j \simeq \alpha_j^{(mod)} (1 + 8\Im\{f_j\}) - 8\Re\{f_j\} \end{cases} \quad , \quad \begin{cases} \frac{1}{\beta_1} (\cot \Delta\phi_{12} + \alpha_1) \\ \frac{1}{\beta_1} (\cot \Delta\phi_{13} + \alpha_1) \end{cases} \quad , \quad (\text{A23})$$

where  $h_{ij}$  and  $f_j$  are the detuning term of Eq. (A18) and the RDT, respectively, corresponding to each plane, whose subscript is omitted here for the sake of notation (the derivation is the same). Before making explicit the two expressions in the above second bracket, the term  $\Re\{f_j - f_i\}$  needs to be evaluated first. From Eq.(4.2)-(4.3) of Ref. [31]  $f_j$  can be rewritten as function of  $f_i$  according to

$$\begin{cases} \hat{h}_{ij} = f_j e^{-i2\phi_j^{(mod)}} - f_i e^{-i2\phi_i^{(mod)}} \Rightarrow f_j = \hat{h}_{ij} e^{i2\phi_j^{(mod)}} + f_i e^{i2\Delta\phi_{ij}^{(mod)}} \\ \hat{h}_{ij} = \mp \frac{1}{8} \sum_{i < w < j} \beta_w^{(mod)} \delta K_{w,1} e^{-i2\phi_w^{(mod)}} \end{cases} \quad , \quad (\text{A24})$$

where again the sum extends over the focusing errors between the two BPMs  $i$  and  $j$  only, while the sign is negative for  $x$ , positive for  $y$ . The label  $i$  shall not be confused with the imaginary unit in the above exponential terms  $i = \sqrt{-1}$ . Hence

$$\begin{aligned} \Re\{f_j - f_i\} &= \Re\left\{ \hat{h}_{ij} e^{i2\phi_j^{(mod)}} + f_i \left( e^{i2\Delta\phi_{ij}^{(mod)}} - 1 \right) \right\} \\ &= \Re\left\{ \hat{h}_{ij} e^{i2\phi_j^{(mod)}} \right\} + |f_i| \Re\left\{ e^{i(2\Delta\phi_{ij}^{(mod)} + q_i)} - e^{iq_i} \right\} \quad q_i \text{ is the phase of } f_i \\ &= \Re\left\{ \hat{h}_{ij} e^{i2\phi_j^{(mod)}} \right\} + |f_i| \left\{ \cos(2\Delta\phi_{ij}^{(mod)} + q_i) - \cos q_i \right\} \\ &= \Re\left\{ \hat{h}_{ij} e^{i2\phi_j^{(mod)}} \right\} + |f_i| \left\{ \cos q_i \left[ \cos 2\Delta\phi_{ij}^{(mod)} - 1 \right] - \sin q_i \sin 2\Delta\phi_{ij}^{(mod)} \right\} \\ &= \Re\left\{ \hat{h}_{ij} e^{i2\phi_j^{(mod)}} \right\} + \Re\{f_i\} \left[ -2 \sin^2 \Delta\phi_{ij}^{(mod)} \right] - \Im\{f_i\} 2 \sin \Delta\phi_{ij}^{(mod)} \cos \Delta\phi_{ij}^{(mod)} \quad . \quad (\text{A25}) \end{aligned}$$

By making use the Taylor expansion of  $\cot(x + \epsilon)$  with  $\epsilon \ll x$ , the BPM phase advance  $\Delta\phi_{ij}$  of Eq. (A23) can be approximated to

$$\cot(x + \epsilon) = \cot x - \frac{\epsilon}{\sin^2 x} + O(\epsilon^2) \quad \Rightarrow \quad \cot \Delta\phi_{ij} \simeq \cot \Delta\phi_{ij}^{(mod)} + \frac{2h_{ij} - 4\Re\{f_j - f_i\}}{\sin^2 \Delta\phi_{ij}^{(mod)}} \quad . \quad (\text{A26})$$



By substituting  $\Re\{f_j - f_i\}$  with Eq. (A25), the above expression reads

$$\cot \Delta\phi_{ij} \simeq \cot \Delta\phi_{ij}^{(mod)} (1 + 8\Im\{f_i\}) + \bar{h}_{ij} + 8\Re\{f_i\} \quad , \quad \bar{h}_{ij} = \frac{2h_{ij} - 4\Re\{\hat{h}_{ij}e^{i2\phi_j^{(mod)}}\}}{\sin^2 \Delta\phi_{ij}^{(mod)}} \quad . \quad (\text{A27})$$

$\bar{h}_{ij}$  can be further made explicit via Eqs. (A11) and (A24), namely

$$\begin{aligned} \bar{h}_{ij} &= \mp \frac{1}{2 \sin^2 \Delta\phi_{ij}^{(mod)}} \sum_{i < w < j} \beta_w^{(mod)} \delta K_{w,1} \left[ 1 - \Re\left\{e^{i2(\phi_j^{(mod)} - \phi_w^{(mod)})}\right\}\right] + O(\delta K_1^2) \\ &= \mp \frac{1}{2 \sin^2 \Delta\phi_{ij}^{(mod)}} \sum_{i < w < j} \beta_w^{(mod)} \delta K_{w,1} \left[ 1 - \cos 2\Delta\phi_{wj}^{(mod)} \right] + O(\delta K_1^2) \\ &= \mp \frac{1}{2 \sin^2 \Delta\phi_{ij}^{(mod)}} \sum_{i < w < j} \beta_w^{(mod)} \delta K_{w,1} 2 \sin^2 \Delta\phi_{wj}^{(mod)} + O(\delta K_1^2) \\ &= \mp \frac{1}{\sin^2 \Delta\phi_{ij}^{(mod)}} \sum_{i < w < j} \beta_w^{(mod)} \delta K_{w,1} \sin^2 \Delta\phi_{wj}^{(mod)} + O(\delta K_1^2) \quad , \end{aligned} \quad (\text{A28})$$

where the sign depends on the plane and the above sum extends over the focusing errors between the two BPMs  $i$  and  $j$ , while  $\Delta\phi_{wj}^{(mod)}$  denotes the phase advance between the BPM  $j$  and the source of error  $w$  of the ideal (or initial) lattice model.

$$\begin{cases} \bar{h}_{x,ij} = -\frac{1}{\sin^2 \Delta\phi_{x,ij}^{(mod)}} \sum_{i < w < j} \beta_{x,w}^{(mod)} \delta K_{w,1} \sin^2 \Delta\phi_{x,wj}^{(mod)} + O(\delta K_1^2) \\ \bar{h}_{y,ij} = +\frac{1}{\sin^2 \Delta\phi_{y,ij}^{(mod)}} \sum_{i < w < j} \beta_{y,w}^{(mod)} \delta K_{w,1} \sin^2 \Delta\phi_{y,wj}^{(mod)} + O(\delta K_1^2) \end{cases} \quad , \quad (\text{A29})$$

All the ingredients are now ready to make explicit the quantities in the most right block of Eq. (A23), by noting that

$$\begin{aligned} \frac{1}{\beta_1} (\cot \Delta\phi_{12} + \alpha_1) &\simeq \frac{\cot \Delta\phi_{12}^{(mod)} (1 + 8\Im\{f_1\}) + \bar{h}_{12} + 8\Re\{f_1\} + \alpha_1^{(mod)} (1 + 8\Im\{f_1\}) - 8\Re\{f_1\}}{\beta_1^{(mod)} (1 + 8\Im\{f_1\})} \\ &\simeq \frac{1}{\beta_1^{(mod)}} \left( \cot \Delta\phi_{12}^{(mod)} + \alpha_1^{(mod)} \right) + \frac{\bar{h}_{12}}{\beta_1^{(mod)} (1 + 8\Im\{f_1\})} \end{aligned} \quad (\text{A30})$$

$$\begin{aligned} &\simeq \frac{1}{\beta_1^{(mod)}} \left( \cot \Delta\phi_{12}^{(mod)} + \alpha_1^{(mod)} \right) + \frac{\bar{h}_{12}}{\beta_1^{(mod)}} + O(\delta K_1^2) \quad , \\ \frac{1}{\beta_1} (\cot \Delta\phi_{13} + \alpha_1) &\simeq \frac{1}{\beta_1^{(mod)}} \left( \cot \Delta\phi_{13}^{(mod)} + \alpha_1^{(mod)} \right) + \frac{\bar{h}_{13}}{\beta_1^{(mod)}} + O(\delta K_1^2) \quad . \end{aligned} \quad (\text{A31})$$

The difference between the above expressions reads

$$\frac{1}{\beta_1} (\cot \Delta\phi_{13} - \cot \Delta\phi_{12}) \simeq \frac{1}{\beta_1^{(mod)}} \left[ (\cot \Delta\phi_{13}^{(mod)} - \cot \Delta\phi_{12}^{(mod)}) + (\bar{h}_{13} - \bar{h}_{12}) \right] + O(\delta K_1^2) \quad , \quad (\text{A32})$$

which is equivalent to

$$\beta_1 \simeq \beta_1^{(mod)} \frac{\cot \Delta\phi_{13} - \cot \Delta\phi_{12}}{(\cot \Delta\phi_{13}^{(mod)} - \cot \Delta\phi_{12}^{(mod)}) + (\bar{h}_{13} - \bar{h}_{12})} + O(\delta K_1^2) \quad , \quad (\text{A33})$$

with  $\bar{h}_{ij}$  defined in Eq. (A29). Eq. (18) is then demonstrated. When no source of focusing error is present between the three BPMs,  $\bar{h}_{13} = \bar{h}_{12} = 0$  and Eq. (15) is retrieved. A special case where Eq. (15) still applies even in the presence of strong localized focusing errors is when  $\bar{h}_{13} = \bar{h}_{12} \neq 0$ . More generally, Eq. (15) remains a robust approximation whenever  $|\bar{h}_{13} - \bar{h}_{12}| \ll |\cot \Delta\phi_{13}^{(mod)} - \cot \Delta\phi_{12}^{(mod)}|$ , or when the beating induced by any quadrupole errors between two BPMs is much smaller than the one generated by focusing glitches along the rest of the ring, i.e.  $|\bar{h}_{12}| \ll |\beta_1^{(mod)} (1 + 8\Im\{f_1\})|$  in Eq. (A30), the RDT  $f_1$  being generated by all sources of error, see Eq. (A2).

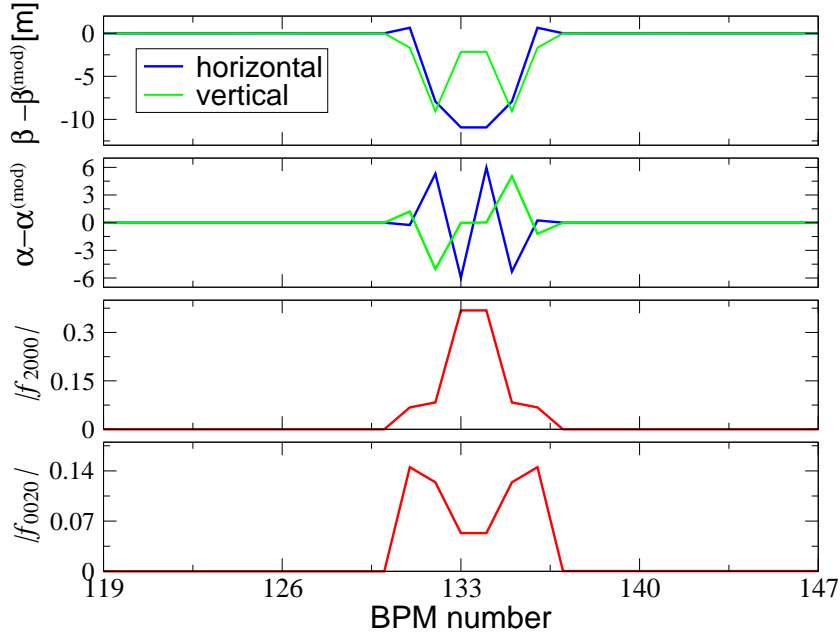


FIG. 9. (Color) Difference between the C-S parameters computed by MADX at the BPMs with and without an example of insertion optics introduced in the lattice of the ESRF storage ring (upper plots). The amplitude of the two corresponding RDTs is plotted in the lower plots, which is zero outside the insertion region. The perfectly matched insertion corresponds hence to a closed RDT bump.

**Interpreting an insertion optics as a closed RDT bump.** Eqs. (A8), (A18), (A22) provide an interesting interpretation of an insertion optics, i.e. of a local modification of the linear optics confined between two points  $i$  and  $j$ , with no change outside.

$$\left\{ \begin{array}{l} \beta_i \simeq \beta_i^{(mod)} (1 + 8\Im\{f_i\}) \\ \alpha_i \simeq \alpha_i^{(mod)} (1 + 8\Im\{f_i\}) - 8\Re\{f_i\} \end{array} \right. , \quad \left\{ \begin{array}{l} \beta_j \simeq \beta_j^{(mod)} (1 + 8\Im\{f_j\}) \\ \alpha_j \simeq \alpha_j^{(mod)} (1 + 8\Im\{f_j\}) - 8\Re\{f_j\} \\ \Delta\phi_{ij} \simeq \Delta\phi_{ij}^{(mod)} - 2h_{ij} + 4\Re\{f_j - f_i\} \end{array} \right. . \quad (\text{A34})$$

If the insertion is perfectly matched to the rest of the machines,  $\beta_i = \beta_j$  and  $\alpha_i = \alpha_j$  (in general the same is true for the dispersion function and its derivative, not discussed here). This implies that: (i)  $f_i = f_j = 0$ , (ii) the RDTs are zero outside the two locations  $i$  and  $j$ , and (iii) the phase advance of the whole insertion is  $\Delta\phi_{ij} = \Delta\phi_{ij}^{(mod)} - 2h_{ij}$ , with  $h_{ij}$  in general nonzero. This in turn implies that the above equations are actually exact, since the remainders proportional to  $|f|^2$  is also zero at the insertion ends. An example of matched insertion optics introduced in the lattice of the ESRF storage ring is showed in Fig. 9, along with the amplitude of the two RDTs. As predicted by Eq. (A34), the RDTs are zero at the ends and outside the insertion region, with a closed bump inside.

**Accurate evaluation of the focusing errors RDTs.** Eqs. (A8), (A17), (A22) compute the C-S parameters modified by focusing errors (or insertion optics) via the corresponding RDTs  $f_{2000}$  and  $f_{0020}$ . They represent already an approximation, linear in RDTs, since terms proportional to higher powers ( $f^2$ ,  $f^3$ , ...) are neglected. For light sources such as the ESRF storage ring, with a typical rms beating of about 3-5% (see top plot of Fig. 1) and ultra-low coupling (the emittance ratio  $\epsilon_y/\epsilon_x$  is about 1‰) this approximation is already rather robust and is expected to be of no concern for more recent machines with the same coupling level and an RMS beating lower than 1%. It remains to asses how reliable is the computation of the RDT from the lattice formula (linear in  $\delta K_1$ ) of Eq. (A2). In Fig. 10 the differences between the C-S parameters computed from an error model (the same of Fig. 1) and from the ideal lattice of the ESRF storage ring are displayed. By taking as reference the values computed by MADX (red curves), an overall good agreement is observed when the lattice formula, Eq. (A2), is used to evaluate the RDTs (green curves), though some local and global discrepancies can be observed: up to 1 m for  $\beta$ , 0.5 for  $\alpha$ , and 5 mrad for the betatron phases  $\phi$ , see Fig. 11.

Fortunately a more accurate way to compute the RDTs exists, though it requires several computational steps. First, single particle tracking is to be performed, with focusing errors included in the lattice and with non-zero initial conditions in both planes, small enough so to remain in the linear regime (a few tens of  $\mu\text{m}$ ). Turn-by-turn position

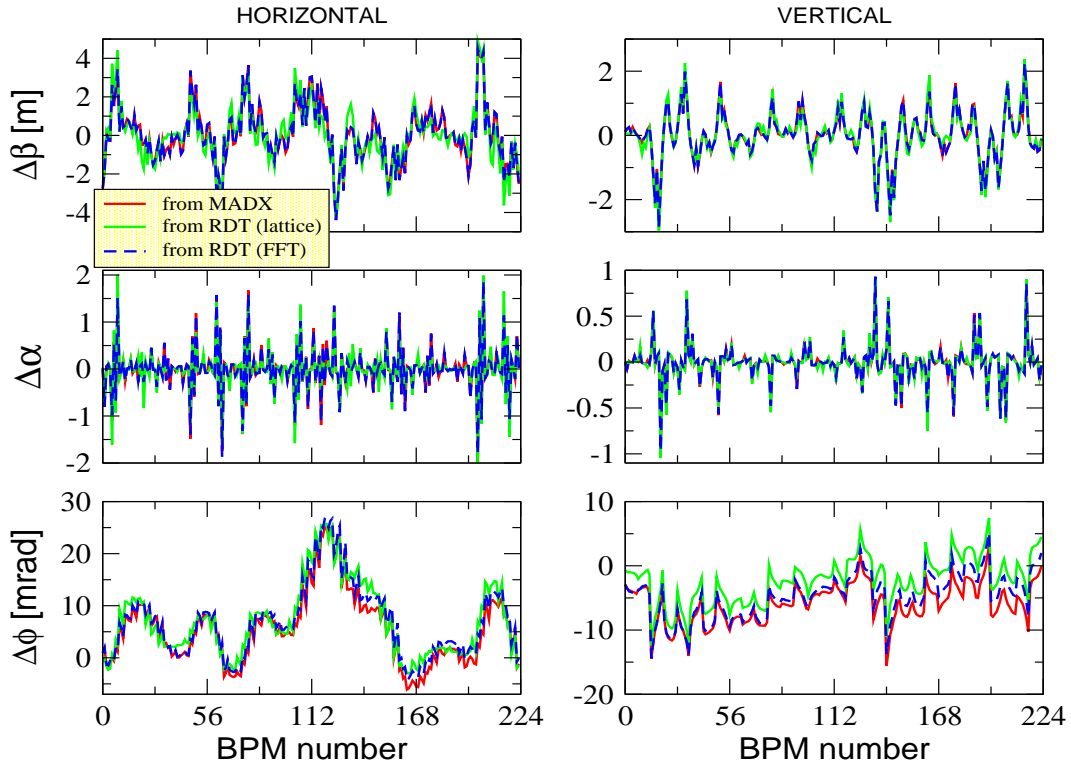


FIG. 10. (Color) Differences between the C-S parameters evaluated from an error model (the same of Fig. 1) and from the ideal lattice of the ESRF storage ring. These differences are computed by MADX (solid red line) and from Eq. (A8) (for  $\beta$ ), Eq. (A22) (for  $\alpha$ ) and Eq. (A17) (for  $\phi$ ). The RDTs in those formulas are computed by the lattice formula (linear in  $\delta K_1$ ) of Eq. (A2) (solid green line) and from Eq. (A36) (FFT of simulated single particle tracking data, dashed blue line).

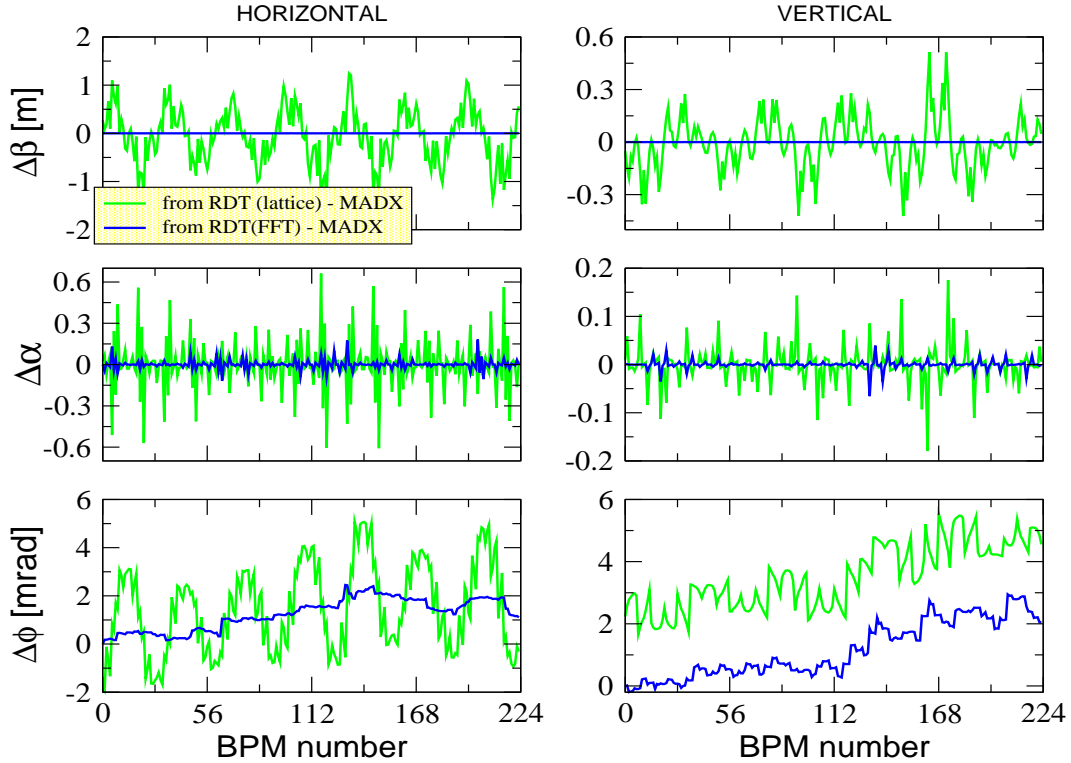


FIG. 11. (Color). Deviations between the change of the C-S parameters computed by MADX and the one predicted by Eq. (A8) (for  $\beta$ ), Eq. (A22) (for  $\alpha$ ) and Eq. (A17) (for  $\phi$ ). The green line is obtained when computing the RDTs via Eq. (A2), whereas the application of Eq. (A36) results in the blue curve, which is much more accurate.

$(x, p_x)$  and momentum  $(y, p_y)$  shall be recorded at the BPMs. The complex C-S variables  $h_x = \tilde{x} - i\tilde{p}_x$  and  $h_y = \tilde{y} - i\tilde{p}_y$  are then computed at each BPM, where the C-S parameters used to convert the Cartesian coordinates are the ones of the ideal model (i.e. without the focusing errors used for tracking). As showed in Appendix C of Ref. [23], from the FFT of  $h_x$  at each BPM two main harmonics can be extracted, one at the tune frequency  $H_h(1, 0)$  and the other at its opposite  $H_h(-1, 0)$  (the same applies to the vertical plane):

$$\begin{aligned} h_x &= \cosh(4|f_{2000}|) \zeta_{x,-} - i \sinh(4|f_{2000}|) e^{iq_{2000}} \zeta_{x,+} , \\ &\quad \uparrow \qquad \qquad \qquad \uparrow \\ &\quad H_h(1, 0) \qquad \qquad H_h(-1, 0) \\ h_y &= \cosh(4|f_{0020}|) \zeta_{y,-} - i \sinh(4|f_{0020}|) e^{iq_{0020}} \zeta_{y,+} , \\ &\quad \uparrow \qquad \qquad \qquad \uparrow \\ &\quad V_h(0, 1) \qquad \qquad V_h(0, -1) \end{aligned} \quad (\text{A35})$$

where  $\zeta_{\pm} = \sqrt{2I} e^{\mp i(2\pi NQ + \phi + \psi_0)}$ . The RDT phase  $q$  and amplitude  $|f|$  can then be inferred from the phase and amplitude of the four lines, according to

$$\begin{cases} q_{2000} = \Phi_{H_h(-1,0)} + \Phi_{H_h(1,0)} + \frac{\pi}{2} \\ q_{0020} = \Phi_{V_h(0,-1)} + \Phi_{V_h(0,1)} + \frac{\pi}{2} \end{cases}, \quad \begin{cases} |f_{2000}| = \frac{1}{4} \operatorname{arctanh} g_x = \frac{1}{8} [\ln(1+g_x) - \ln(1-g_x)] , \quad g_x = \frac{|H_h(-1,0)|}{|H_h(1,0)|} \\ |f_{0020}| = \frac{1}{4} \operatorname{arctanh} g_y = \frac{1}{8} [\ln(1+g_y) - \ln(1-g_y)] , \quad g_y = \frac{|V_h(0,-1)|}{|V_h(0,1)|} \end{cases} . \quad (\text{A36})$$

By using the RDTs inferred from the above FFT formulas in Eqs. (A8), (A17), (A22), the agreement with the C-S parameters computed by MADX is greatly improved, as showed by the blue curves of Figs. 10 and 11: The accuracy is better than 1 mm for  $\beta$ , 0.15 for  $\alpha$ , and up 3 mrad for  $\phi$ . When computing the BPM phase advance error, the deviation drops to about 0.1 mrad. The accumulation of inaccuracy for  $\phi$  along the ring (bottom plot of Fig. 11) can be attributed to higher-order terms in the computation of  $h_{ij}$  and nonlinear terms put in the remainder  $O(|f|^2)$  of Eq. (A18).

**Evaluating the beta beating from the tune line amplitude.** From Eqs. (A3)-(A4) the tune line amplitude at the BPM  $j$  reads

$$|H(1,0)_j| = \frac{C_{x,j}}{2} \sqrt{2I_x} A_{f,j} \quad , \quad C_{x,j} = 1 + \mathcal{E}_{x,j} \quad , \quad 0 \simeq \mathcal{E}_{x,j} \ll 1 \quad , \quad (\text{A37})$$

where the BPM calibration factor is included and represented by a small calibration error  $\mathcal{E}_{x,j}$  for a later perturbative expansion. By averaging over all BPMs the following expression for the invariant is obtained

$$\langle |H(1,0)| \rangle = \frac{\langle C_x \rangle}{2} \sqrt{2I_x} \langle A_f \rangle \quad \Rightarrow \quad \sqrt{2I_x} = \frac{2 \langle |H(1,0)| \rangle}{\langle C_x \rangle \langle A_f \rangle} \quad , \quad (\text{A38})$$

$C$  and  $A_f$  being uncorrelated quantities. On the other hand,  $A_{f,j}$  can be written as the ratio between the real beta and the ideal one, see Eq. (11),

$$A_{f,j} = \sqrt{\frac{\beta_{x,j}}{\beta_{x,j}^{(mod)}}} \quad \Rightarrow \quad |H(1,0)_j| = \frac{C_{x,j}}{2} \sqrt{2I_x} \sqrt{\frac{\beta_{x,j}}{\beta_{x,j}^{(mod)}}} \quad \Rightarrow \quad \beta_{x,j} = \beta_{x,j}^{(mod)} \frac{2|H(1,0)_j|^2}{C_{x,j}^2 (2I_x)} . \quad (\text{A39})$$

By replacing  $(2I_x)$  with the expression of Eq. (A38), the above expression reads

$$\beta_{x,j} = \beta_{x,j}^{(mod)} \left( \frac{|H(1,0)_j|}{\langle |H(1,0)| \rangle} \right)^2 \left( \frac{\langle C_x \rangle}{C_{x,j}} \right)^2 \langle A_f \rangle^2 . \quad (\text{A40})$$

The last two terms in the r.h.s of the above equation can be approximated by

$$\begin{cases} \left( \frac{\langle C_x \rangle}{C_{x,j}} \right)^2 = \left( \frac{1 + \langle \mathcal{E}_x \rangle}{1 + \mathcal{E}_{x,j}} \right)^2 \simeq (1 + \langle \mathcal{E}_x \rangle - \mathcal{E}_{x,j} + O(\mathcal{E}_x^2))^2 \simeq 1 + 2(\langle \mathcal{E}_x \rangle - \mathcal{E}_{x,j}) + O(\mathcal{E}_x^2) \\ \langle A_f \rangle^2 \simeq \langle 1 + 32|f_{2000}|^2 + 8|f_{2000}| \sin q_{2000} + O(|f_{2000}|^3) \rangle^{-2} \simeq 1 + 64 \langle |f_{2000}|^2 \rangle + O(|f_{2000}|^3) \end{cases} . \quad (\text{A41})$$

Eq. (A40) then becomes

$$\begin{cases} \beta_{x,j} = \beta_{x,j}^{(mod)} \left( \frac{|H(1,0)_j|}{\langle |H(1,0)| \rangle} \right)^2 [1 + 2(\langle \mathcal{E}_x \rangle - \mathcal{E}_{x,j}) + O(\mathcal{E}_x^2)] [1 + 64 \langle |f_{2000}|^2 \rangle + O(|f_{2000}|^3)] \\ \beta_{y,j} = \beta_{y,j}^{(mod)} \left( \frac{|V(0,1)_j|}{\langle |V(0,1)| \rangle} \right)^2 [1 + 2(\langle \mathcal{E}_y \rangle - \mathcal{E}_{y,j}) + O(\mathcal{E}_y^2)] [1 + 64 \langle |f_{0020}|^2 \rangle + O(|f_{0020}|^3)] \end{cases} , \quad (\text{A42})$$



where the expression for the vertical plane is obtained with the same derivation.  $\langle \mathcal{E} \rangle$  and  $\langle |f|^2 \rangle$  represent the averaged values (over all BPMs) of the calibration errors and of the amplitudes of the RDTs, respectively. Unless these are determined by independent measurements, they cannot be disentangled and are not observable. A (rude) zero-order truncation is then needed in order to apply Eq. (A42) to real data, yielding to

$$\begin{cases} \beta_{x,j} = \beta_{x,j}^{(mod)} \left( \frac{|H(1,0)_j|}{\langle |H(1,0)| \rangle} \right)^2 + O(\mathcal{E}_x, |f_{2000}|^2) \\ \beta_{y,j} = \beta_{y,j}^{(mod)} \left( \frac{|V(0,1)_j|}{\langle |V(0,1)| \rangle} \right)^2 + O(\mathcal{E}_y, |f_{0020}|^2) \end{cases} \quad (\text{A43})$$

## Appendix B: Impact of octupolar-like terms on the tune lines: an amplitude dependent focusing

All results of Appendix A and Sec. II are valid as long as the beam motion remains in the linear regime, i.e. nonlinear terms may be neglected. In this appendix this assumption is removed and the extension of Eq. (10) to include higher-order contributions is derived. The result will be a more complicated formula with additional terms dependent on the initial oscillation amplitudes ( $2I_{x,y}$ ), both in the tune line amplitude and phase. These are proportional to octupolar fields ( $\propto K_3$ ) and to quadratic functions of sextupole strengths ( $\propto K_2^2$ ).

In Table V-VII of Ref. [30] the list of secondary harmonics of the the complex signals  $h_x = \tilde{x} - i\tilde{p}_x$  and  $h_y = \tilde{y} - i\tilde{p}_y$  generated by octupolar-like RDTs is presented. It can be seen how their spectral lines  $H_h(-1, 0)$  and  $V_h(0, -1)$ , which in the linear regime are excited only by focusing errors via the two quadrupolar RDTs  $f_{2000}$  and  $f_{0020}$ , respectively, receive a contribution from several octupolar-like RDTs too. To the first order in the RDTs, these lines read

$$\begin{cases} H_h(-1, 0) = \left[ -4i\sqrt{2I_x}f_{2000} - 6i(2I_x)f_{3100} - 4i\sqrt{(2I_x)(2I_y)}f_{2011} + O(f^2, I^2) \right] e^{-\tau_x} \\ V_h(0, -1) = \left[ -4i\sqrt{2I_y}f_{0020} - 6i(2I_y)f_{0031} - 4i\sqrt{(2I_x)(2I_y)}f_{1120} + O(f^2, I^2) \right] e^{-\tau_y} \\ \tau_x = i \left\{ 2\pi N \left[ Q_x^{(mod)} - 2h_{1100} - 4h_{2200}(2I_x) - 2h_{1111}(2I_y) + O(I^2) \right] + \phi_x + \psi_{x0} \right\} \\ \tau_y = i \left\{ 2\pi N \left[ Q_y^{(mod)} - 2h_{0011} - 4h_{0022}(2I_y) - 2h_{1111}(2I_x) + O(I^2) \right] + \phi_y + \psi_{y0} \right\} \end{cases} \quad (\text{B1})$$

The above expressions are derived from the more general expression for the TBT complex signals [30]

$$\begin{cases} h_x(N) = \sqrt{2I_x} e^{i(2\pi Q_x N + \phi_x + \psi_{x0})} - 2i \sum_{pqrt} p f_{pqrt} (2I_x)^{\frac{p+q-1}{2}} (2I_y)^{\frac{r+t}{2}} e^{i[(1-p+q)(2\pi Q_x N + \phi_x + \psi_{x0}) + (t-r)(2\pi Q_y N + \phi_y + \psi_{y0})]} \\ h_y(N) = \sqrt{2I_y} e^{i(2\pi Q_y N + \phi_y + \psi_{y0})} - 2i \sum_{pqrt} r f_{pqrt} (2I_x)^{\frac{p+q}{2}} (2I_y)^{\frac{r+t-1}{2}} e^{i[(q-p)(2\pi Q_x N + \phi_x + \psi_{x0}) + (1-r+t)(2\pi Q_y N + \phi_y + \psi_{y0})]} \end{cases} \quad (\text{B2})$$

The harmonic  $H_h(-1, 0)$  ( $V_h(0, -1)$ ) is the sum of all terms in the above summation such that  $1 - p + q = -1$  and  $t - r = 0$  ( $q - p = 0$  and  $1 - r + t = -1$ ), i.e. all those oscillating with the opposite betatron tune and phase. The first term, scaling with  $\sqrt{2I}$ , is then  $f_{2000}$ , as  $1 - 2 + 0 = -1$  and  $0 - 0 = 0$  ( $f_{0020}$ , since  $0 - 0 = 0$  and  $1 - 2 + 0 = -1$ ). Following the same logic, the next terms in  $H_h(-1, 0)$  scaling with  $(2I_x)$  are  $f_{3100}$ , ( $1 - 3 + 1 = -1$  and  $0 - 0 = 0$ ) and  $f_{2011}$  ( $1 - 2 + 0 = -1$  and  $1 - 1 = 0$ ). The same rule applied to  $V_h(0, -1)$  selects  $f_{0031}$  and  $f_{1120}$ . All last four RDTs are normal octupolar-like ( $f_{pqrt}$ , with  $p + q + r + t = 4$ ), with  $f_{3100}$  and  $f_{0031}$  excited by the potential terms  $\propto x^4$  and  $y^4$ , respectively, whereas both  $f_{2011}$  and  $f_{1120}$  stem from the monomial  $\propto x^2 y^2$ . Detuning terms  $h$  are those elements of the complex C-S Hamiltonian

$$\tilde{H} = \sum_n \sum_{pqrt}^{n=p+q+r+t} h_{pqrt} (2I_x)^{\frac{p+q}{2}} (2I_y)^{\frac{r+t}{2}} e^{i[(p-q)(\phi_x + \psi_{x0}) + (r-t)(\phi_y + \psi_{y0})]} \quad , \quad (\text{B3})$$

that do not depend on the betatron phase, i.e.  $p = q$  and  $r = t$ . In the above definition  $n$  represents the multipole order (normal and skew):  $n = 2$  for quadrupoles,  $n = 3$  for sextupoles,  $n = 4$  for octupole, etc. The explicit formula for  $h_{pqrt}$  reads

$$\begin{aligned} h_{pqrt} &= - \frac{[K_{n-1}\Omega(r+t) + iJ_{n-1}\Omega(r+t+1)]}{p! \ q! \ r! \ r! \ 2^{p+q+r+t}} i^{r+t} (\beta_x)^{\frac{p+q}{2}} (\beta_y)^{\frac{r+t}{2}} \ , \\ \Omega(i) &= 1 \text{ if } i \text{ is even, } \quad \Omega(i) = 0 \text{ if } i \text{ is odd} \quad . \end{aligned} \quad (\text{B4})$$

$\Omega(i)$  is introduced to select either the normal or the skew multipoles.  $K_{n-1}$  and  $J_{n-1}$  are the integrated magnet strengths of Eq. (7). If several sources are to be included in the above Hamiltonian, a further summation taking into account the relative phase advances between magnets and observation point needs to be included in Eq. (B3), see Appendix A of Ref. [23].

The RDT  $f_{pqrt}$  and the detuning terms  $h_{pprr}$  introducing a dependence on the initial amplitude ( $2I$ ) in Eq. (B1) are proportional to the octupolar strengths ( $\propto K_3$ , generated either by physical octupole magnets or by octupolar components of other magnets) and to quadratic functions of sextupole strengths ( $\propto K_2^2$ ).

Nonlinear terms affect the tune lines (of the complex signals). According to Eqs.(C29)-(C30) of Ref. [23] these read

$$\begin{cases} H_h(1, 0) = \sqrt{2I_x} [1 + T_{H_x}(2I_x) + T_{H_y}(2I_y) + O((2I_{x,y})^2)] e^{\tau_x} \\ V_h(0, 1) = \sqrt{2I_y} [1 + T_{V_x}(2I_x) + T_{V_y}(2I_y) + O((2I_{x,y})^2)] e^{\tau_y} \end{cases}, \quad (\text{B5})$$

where the complex functions  $T$  are quadratic functions of the sextupole strengths ( $\propto K_2^2$ ) and the expansion is truncated to the first non-zero terms of the invariants. These four spectral lines can be conveniently rewritten as

$$\begin{cases} H_h(1, 0) = \sqrt{2I_x} [1 + T_H(K_2^2, I_{x,y})] e^{\tau_x} \\ V_h(0, 1) = \sqrt{2I_y} [1 + T_V(K_2^2, I_{x,y})] e^{\tau_y} \\ H_h(-1, 0) = -i\sqrt{2I_x} [4f_{2000} + F_{xx}^*(K_2^2, K_3, I_{x,y})] e^{-\tau_x} \\ V_h(0, -1) = -i\sqrt{2I_y} [4f_{0020} + F_{yy}^*(K_2^2, K_3, I_{x,y})] e^{-\tau_y} \end{cases}, \quad (\text{B6})$$

where the remainders  $O(f^2, I^2)$  have been ignored. The dependence of the complex and longitudinally varying functions  $T$  and  $F$  on the magnetic strengths  $K_{2,3}$  is indicated in the parenthesis. Since the harmonic analysis is performed here on the real signals  $\tilde{x}$  and  $\tilde{y}$ , the observable tune lines read

$$\begin{cases} H(1, 0) = \frac{1}{2}[H_h(1, 0) + H_h^*(-1, 0)] = \frac{\sqrt{2I_x}}{2} [1 + 4if_{2000}^* + iF_{xx}(K_2^2, K_3, I_{x,y}) + T_H(K_2^2, I_{x,y})] e^{\tau_x} \\ V(0, 1) = \frac{1}{2}[V_h(0, 1) + V_h^*(0, -1)] = \frac{\sqrt{2I_y}}{2} [1 + 4if_{0020}^* + iF_{yy}(K_2^2, K_3, I_{x,y}) + T_V(K_2^2, I_{x,y})] e^{\tau_y} \end{cases}. \quad (\text{B7})$$

The generalization of the tune line amplitude and phase of Eq. (11) at a BPM  $j$  in the nonlinear (amplitude dependent) regime are then

$$\begin{cases} |H(1, 0)_j| = \frac{\sqrt{2I_x}}{2} |B_{x,j}|, & \Phi_{H(1,0),j} = \phi_{x,j}^{(mod)} + \psi_{x0} + \arg\{B_{x,j}\} - 2h_{1100,j} - 4h_{2200,j}(2I_x) - 2h_{1111,j}(2I_y) \\ |V(0, 1)_j| = \frac{\sqrt{2I_y}}{2} |B_{y,j}|, & \Phi_{V(0,1),j} = \phi_{y,j}^{(mod)} + \psi_{y0} + \arg\{B_{y,j}\} - 2h_{0011,j} - 2h_{1111,j}(2I_x) - 4h_{0022,j}(2I_y) \\ B_{x,j} = 1 + i4f_{2000,j}^* + iF_{xx,j}(K_2^2, K_3, I_{x,y}) + T_{H,j}(K_2^2, I_{x,y}) \\ B_{y,j} = 1 + 4if_{0020,j}^* + iF_{yy,j}(K_2^2, K_3, I_{x,y}) + T_{V,j}(K_2^2, I_{x,y}) \end{cases}. \quad (\text{B8})$$

The linear regime may be then defined as the range of initial oscillation amplitudes, i.e. of  $2I_{x,y}$ , such that the functions  $F$ ,  $T$  may be ignored along with the amplitude dependent detuning terms  $h_{2200,j}$ ,  $h_{1111,j}$  and  $h_{0022,j}$ . These are defined as the summation of all octupolar-like sources from the beginning of the ring up to the BPM  $j$ , in the same way  $h_{1100,j}$  and  $h_{0011,j}$  were defined in Eq. (A14) and are non-zero even if the global detuning with amplitude is zero or negligible. The generalization of observable BPM phase advance of Eq. (14) eventually reads

$$\begin{aligned} \Delta\Phi_{H,ij} &= \Delta\phi_{x,ij}^{(mod)} + \arg\{B_{x,i} - B_{x,j}\} - 2h_{1100,ij} - 4h_{2200,ij}(2I_x) - 2h_{1111,ij}(2I_y) \\ \Delta\Phi_{V,ij} &= \Delta\phi_{y,ij}^{(mod)} + \arg\{B_{y,i} - B_{y,j}\} - 2h_{0011,ij} - 2h_{1111,ij}(2I_x) - 4h_{0022,ij}(2I_y) \end{aligned}, \quad (\text{B9})$$

where the the subscript  $ij$  in the detuning terms  $h_{pqrt,ij}$  means that only the summation of detuning sources between the two BPMs  $i$  and  $j$  is to be taken into account, as in Eq. (A18) for the linear case.

In conclusion, if the initial oscillation amplitude ( $2I$ ) is *too large*, the betatron BPM phase advance  $\Delta\phi_{ij}$  is no longer measurable from the difference of the tune line phases  $\Delta\Phi_{ij}$ , since amplitude dependent focusing, octupolar-like, resonant and detuning terms *corrupt* the tune line. The same is true for the invariant itself ( $2I$ ), which is no longer measurable from the tune line amplitude. The latter is no longer constant along the ring and its modulation depends on the invariant itself via the functions  $F$  and  $T$  of Eq. (B8).

### Appendix C: Impact of octupolar-like terms on the coupling lines: an amplitude dependent coupling

Octupolar-like RDTs do not contribute to the tunes lines only, but to several other harmonics of the complex TBT signals, including the coupling lines. By applying the same procedure presented in Appendix B, the contributions to the harmonic  $H_h(0, \pm 1)$  ( $V_h(\pm 1, 0)$ ) are all terms in the summation of Eq. (B2) such that  $1 - p + q = 0$  and  $t - r = \pm 1$  ( $q - p = \pm 1$  and  $1 - r + t = 0$ ). The result is

$$\begin{cases} H_h(0, 1) = -2i [f_{1001} + 2(2I_x)f_{2101} + (2I_y)f_{1012} + O(f^2, I^2)] \sqrt{2I_y} e^{\tau_y} \\ H_h(0, -1) = -2i [f_{1010} + 2(2I_x)f_{2110} + (2I_y)f_{1021} + O(f^2, I^2)] \sqrt{2I_y} e^{-\tau_y} \end{cases}, \quad (C1)$$

$$\begin{cases} V_h(1, 0) = -2i [f_{1001}^* + (2I_x)f_{2101}^* + 2(2I_y)f_{1012}^* + O(f^2, I^2)] \sqrt{2I_x} e^{\tau_x} \\ V_h(-1, 0) = -2i [f_{1010} + (2I_x)f_{2110} + 2(2I_y)f_{1021} + O(f^2, I^2)] \sqrt{2I_x} e^{-\tau_x} \end{cases}.$$

The amplitude dependent coupling is then generated by skew octupolar-like RDTs, with  $f_{2101}$  and  $f_{2110}$  excited by the  $x^3y$  potential term, while  $f_{1012}$  and  $f_{1021}$  originate from the  $xy^3$  monomial. Note that in the above equations the relation  $f_{pqrt} = f_{qptr}^*$  is used here for simplicity, though it is not strictly true when second order terms are to be taken into account: See Appendix A of Ref. [23]. The coupling lines of the real signals  $\tilde{x}$  and  $\tilde{y}$ , then read

$$\begin{cases} H(0, 1) = \frac{1}{2} [H_h(0, 1) + H_h^*(0, -1)] = -i [F_{xy}(J_1) + T_{xy}(J_3, K_3, K_2^2, J_1, I_{x,y})] \sqrt{2I_y} e^{\tau_y} \\ V(1, 0) = \frac{1}{2} [V_h(1, 0) + V_h^*(-1, 0)] = -i [F_{yx}(J_1) + T_{yx}(J_3, K_3, K_2^2, J_1, I_{x,y})] \sqrt{2I_x} e^{\tau_x}, \\ F_{xy} = f_{1001} - f_{1010} \quad , \quad T_{xy} = 2(f_{2101} - f_{2110}^*)(2I_x) + (f_{1012} - f_{1021}^*)(2I_y) \\ F_{yx} = f_{1001}^* - f_{1010}^* \quad , \quad T_{yx} = (f_{2101}^* - f_{2110}^*)(2I_x) + 2(f_{1012}^* - f_{1021}^*)(2I_y) \end{cases}, \quad (C2)$$

where the remainders  $O(f^2, I^2)$  have been ignored.  $F_{xy}$  and  $F_{yx}$  are the same of Eq. (16) and generate betatron coupling, which is amplitude independent.  $T_{xy}$  and  $T_{yx}$  are instead responsible for the amplitude dependent coupling and can be excited by several sources. To the first order they are generated by skew octupole fields  $J_3$ , and by cross terms  $\propto K_3 \otimes J_1$  (i.e. between normal octupole and skew quadrupole) to the second order.  $J_3$  in turn can stem from the cross product  $\propto K_2 \otimes J_2$  (i.e. between normal and skew sextupole), with  $J_2$  originating from another cross term  $\propto K_2 \otimes J_1$ .  $K_3$  is also created by a last cross term  $\propto K_2 \otimes K_2$ . In summary, the following scaling laws may be drafted:

$$J_3 \leftrightarrow (K_3) \otimes J_1, \quad K_2 \otimes [J_2] \leftrightarrow (K_2 \otimes K_2) \otimes J_1, \quad K_2 \otimes [K_2 \otimes J_1] \leftrightarrow K_2 \otimes K_2 \otimes J_1, \quad (C3)$$

$$K_3 \otimes J_1 \leftrightarrow K_2 \otimes K_2 \otimes J_1. \quad (C4)$$

Hence,  $T_{xy}$  and  $T_{yx}$  are nonzero even in the absence of physical normal or skew octupoles and scale quadratically with the sextupole strength  $K_2$  and linearly with the skew quadrupole field  $J_1$ . Since the betatron coupling terms  $F_{xy}$  and  $F_{yx}$  scale linearly with  $J_1$ , the overall amplitude dependent modulation of the coupling lines scales quadratically with the sextupole fields, i.e. with the same order of magnitude of the tune line modulation of Eq. (B8).

Amplitude and phase of the coupling lines at a generic BPM  $j$  are eventually derived from Eq. (C2), resulting in

$$\begin{cases} |H(0, 1)_j| = |F_{xy,j}(J_1) + T_{xy,j}(J_3, K_3, K_2^2, J_1, I_{x,y})| \sqrt{2I_y} \\ |V(1, 0)_j| = |F_{yx,j}(J_1) + T_{yx,j}(J_3, K_3, K_2^2, J_1, I_{x,y})| \sqrt{2I_x} \\ \arg \{H(0, 1)_j\} = \phi_{x,j} + \psi_{x0} + \arg \{F_{xy,j} + T_{xy,j}\} - \frac{\pi}{2} \\ \arg \{V(1, 0)_j\} = \phi_{y,j} + \psi_{y0} + \arg \{F_{yx,j} + T_{yx,j}\} - \frac{\pi}{2} \end{cases}. \quad (C5)$$

- 
- [1] M. Minty and F. Zimmermann, *Measurement and Control of Charged Particle Beams*, Springer, Berlin, 2003 (ISBN 3-540-44197-5).  
[2] J. Borer, A. Hofmann, J.-P. Koutchouk, T. Risselada, B. Zotter, CERN/LEP/ISR/83-12 (1983).  
[3] P. Castro García, PhD thesis, p.49, CERN-SL-96-070-BI

- (1996).  
[4] P. Castro García, J. Borer, A. Burns, G. Morpurgo, R. Schmidt, Proceedings of PAC 1993, p 2103 (1993).  
[5] Y.T. Yan, Y. Cai, W. Colocho, F.-J. Decker, J. Seeman, M. Sullivan, J. Turner, U. Wienands, M. Woodley, G. Yocky, SLAC-PUB-11925 (2006).

- [6] D. Sagan, R. Meller, R. Littauer, and D. Rubin, Phys. Rev. ST Accel. Beams **3**, 092801 (2000)
- [7] Akio Morita, Haruyo Koiso, Yukiyoishi Ohnishi, Katsunobu Oide, Phys. Rev. ST Accel. Beams **10**, 072801 (2007)
- [8] J. Safranek, Nucl. Instr. and Meth. A, vol. **388**, pp. 27-36 (1996).
- [9] *ICFA BD Newsletter*, edited by A. Ghodke (ICFA Beam Dynamics Panel, 2007), No. 44 .
- [10] J. Irwin, C. X. Wang, Y. T. Yan, K. L. F. Bane, Y. Cai, F.-J. Decker, M. G. Minty, G. V. Stupakov, F. Zimmermann, Phys. Rev. Lett. **82**, 1684 (1999).
- [11] X. Huang, S.Y. Lee, E. Prebys, R. Tomlin, Phys. Rev. ST Accel. Beams **8**, 064001 (2005)
- [12] M. Carlá, Z. Martí, G. Benedetti, L. Nadolski, Proceedings of the International Particle Accelerator Conference, IPAC2015, Richmond, VA, USA, 2015, p. 1686.
- [13] A. Langner, G. Benedetti, M. Carlá, J. Coello de Portugal, U. Iriso, Z. Martí, R. Tomás, Proceedings of IPAC2015, Richmond, VA, USA, p. 430 (2015).
- [14] Z. Martí, CELLS ALBA note, ACDIV-2013-17 (2013)
- [15] M. Aiba, M. Böge, J. Chrin, N. Milas, T. Schilcher, and A. Streun, Phys. Rev. ST Accel. Beams **16**, 012802 (2013).
- [16] G. Rehm, M.G. Abbott, A.F. D. Morgan, J. Rowland, I. Uzun, Proceedings of Beam and Instrumentation Workshop BIW2010, Santa Fe, New Mexico USA, 2010.
- [17] W. Herr, F. Schmidt, CERN AB Note, CERN-AB-2004-027-ABP (2004).
- [18] A. Terebilo, Proceedings of PAC01, p 3203, Chicago, Illinois, USA (2001).
- [19] A. Langner and R. Tomás, Phys. Rev. ST Accel. Beams,**18**, 031002 (2015).
- [20] T. Persson and R. Tomás, Phys. Rev. ST Accel. Beams,**17**, 051004 (2014).
- [21] A. Franchi, E. Métral, and R. Tomás García, Phys. Rev. ST Accel. Beams, vol. **10**, 064003 (2007).
- [22] A. Franchi, L. Farvacque, J. Chavanne, F. Ewald, B. Nash, K. Scheidt and R. Tomás, Phys. Rev. ST Accel. Beams, vol. **14**, 034002, (2011).
- [23] A. Franchi, L. Farvacque, F. Ewald, G. Le Bec and K. B. Scheidt, <http://arxiv.org/abs/1402.1461>. A. Franchi, L. Farvacque, F. Ewald, G. Le Bec and K. B. Scheidt, Phys. Rev. ST Accel. Beams, vol. **17**, 074001, (2013).
- [24] R. Bartolini, A. Bazzani, M. Giovannozzi, W. Scandale and E. Todesco, CERN SL/95-84 (AP) (1995).
- [25] R. Tomás García, Ph.D. thesis, University of Valencia, (Report No. CERN-THESIS-2003-010, 2003)
- [26] C. X. Wang, Stanford Ph.D. dissertation (1999), also SLAC-R-547
- [27] C. X. Wang, V. Sajaev, and C. Y. Yao, Phys. Rev. ST Accel. Beams, vol. **6**, 104001,(2003).
- [28] X. Shen, S. Y. Lee, M. Bai, S. White, G. Robert-Demolaize, Y. Luo, A. Marusic, and R. Tomás, Phys. Rev. ST Accel. Beams **16**, 111001 (2013) and references therein.
- [29] D. D. Caussyn, M. Ball, B. Brabson, J. Collins, S. A. Curtis, V. Derenchuck, D. DuPlantis, G. East, M. Ellison, T. Ellison, D. Friesel, B. Hamilton, W. P. Jones, W. Lambie, S. Y. Lee, D. Li, M. G. Minty, T. Sloan, G. Xu, A. W. Chao, K. Y. Ng, and S. Tepikian, Phys. Rev. A **46**, 7942 (1992).
- [30] R. Bartolini and F. Schmidt, LHC Project note 132 (revised 3<sup>rd</sup> revision May 2005), Part. Accelerators. **59**, pp. 93-106, (1998).
- [31] A. Franchi, PhD thesis, GSI DISS 2006-07 (2006). Ph.D. thesis, J.W. Goethe University (Report No. GSI DISS 2006-07, 2006).
- [32] G. Rehm, Proceedings of the European Particle Accelerator Conference EPAC08, Genoa, Italy, 2008, p. 1016.
- [33] S. Xu, G. Decker, H. Bui, H. Shang, F.R. Lenkszus, R. Laird, C. Yao, Proceedings of the International Particle Accelerator Conference, IPAC10, Kyoto, Japan, 2010, p. 1176
- [34] R.E. Meller, A.W. Chao, J.M. Peterson, S.G. Peggs, M. Furman, Technical Report SSC-N-360, SSCL, 1987.
- [35] S.Y. Lee, Technical Report SSC-N-749, SSCL, 1991.
- [36] A. Sargsyan, Nucl. Instr. and Meth. A, vol. **638**, pp. 15-18 (2011).